ETH zürich

ETH Library

Modeling distributed metal pollution transport in a mine impacted catchment: Short and long-term effects

Journal Article

Author(s):
Sui, Chunming; Fatichi, Simone; Burlando, Paolo; Weber, Enrico; Battista, Giulia

Publication date:
2022-03-15

Permanent link:
https://doi.org/https://doi.org/10.3929/ethz-b-000519856

Rights / license:
Creative Commons Attribution-NonCommercial-NoDerivatives 4.0 International

Originally published in:
Science of The Total Environment 812, https://doi.org/10.1016/j.scitotenv.2021.151473

This page was generated automatically upon download from the ETH Zurich Research Collection.
For more information, please consult the Terms of use.

Science of the Total Environment 812 (2022) 151473

Contents lists available at ScienceDirect

Science of the Total Environment

journal homepage: www.elsevier.com/locate/scitotenv

Modeling distributed metal pollution transport in a mine impacted catchment: Short and long-term effects

Chunming Sui [a,b,*], Simone Fatichi [c], Paolo Burlando [a], Enrico Weber [a,d], Giulia Battista [a]

[a] Swiss Federal Institute of Technology, ETH Zurich, Department of Civil, Environmental and Geomatic Engineering, Institute of Environmental Engineering, Hydrology and Water Resources Management, Stefano-Franscini-Platz 5, 8093 Zurich, Switzerland
[b] Swiss Federal Institute of Technology, ETH Zurich, Department of Humanities, Social and Political Sciences, Institute of Science, Technology, and Policy (ISTP), Universitätstrasse 41, 8092 Zurich, Switzerland
[c] Department of Civil and Environmental Engineering, National University of Singapore, Singapore
[d] SoftWater s.r.l., Via G. Luosi 13, 20131 Milano, Italy

HIGHLIGHTS

- A distributed trace metal transport and transformation module was coupled with TOPKAPI-ETH.
- The model simulates transport of suspended sediment and associated trace metals.
- The model is used to explore the effect of human intervention on C-Q relationships.
- High amount of trace metal with suspended sediment may not imply a high ecological risk.

GRAPHICAL ABSTRACT

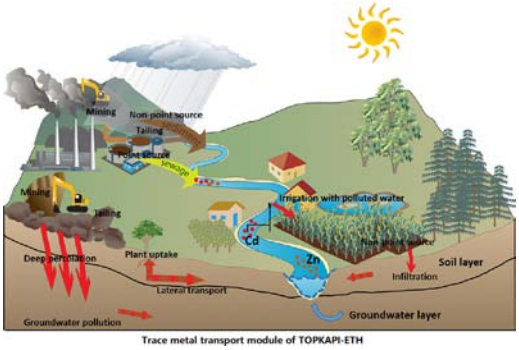

Trace metal transport module of TOPKAPI-ETH

ARTICLE INFO

Article history:
Received 19 July 2021
Received in revised form 29 October 2021
Accepted 2 November 2021
Available online 4 November 2021

Editor: Filip M.G. Tack

Keywords:
Mining pollution
Distributed hydrological model
Trace metal
Catchment transport process
Pollution risk management

ABSTRACT

A spatially distributed trace metal transport and transformation module was developed and implemented within the hydrological model TOPKAPI-ETH. The new module can be used to better understand, at high spatial and temporal resolution, the transport and reactions of trace metals as they move through a catchment from upland sources to downstream areas and water bodies. The newly developed module takes into consideration solid metal in multiple chemical phases with different reactivity and simulates their mutual transformation over time, which gives the possibility to analyze the fraction of different solid metal phases present in the river suspended sediment. The characteristics and potential of the model are demonstrated by simulating Zinc (Zn) and Cadmium (Cd) dynamics in a headwater catchment of the Xiang River in South China, which has been highly perturbed by mining activities. The developed module is shown to reasonably reproduce the observed dynamics of dissolved and total trace metals flux for 14 months at two monitoring stations. The distributed solute transport model was proved to be capable of explaining the reasons underlying the spatial variability of C-Q relationships that are driven by the combined effect of point and non-point pollution sources, as well as identifying the spatio-temporal hotspots of trace metal pollution. By means of synthetic numerical experiments, a limited impact of slow reactions on dissolved Cd transport from upland to river over short-temporal scales was demonstrated, while for longer scales, e.g. >5 years, this effect becomes more relevant, highlighting potential long-lasting sources of trace metal pollution and their impacts.
© 2021 The Authors. Published by Elsevier B.V. This is an open access article under the CC BY-NC-ND license (http://creativecommons.org/licenses/by-nc-nd/4.0/).

* Corresponding author at: UNO D 12, Institute of Science, Technology, and Policy (ISTP), Universitätstrasse 41, 8092 Zurich, Switzerland.
E-mail address: chunming.sui@istp.ethz.ch (C. Sui).

https://doi.org/10.1016/j.scitotenv.2021.151473
0048-9697/© 2021 The Authors. Published by Elsevier B.V. This is an open access article under the CC BY-NC-ND license (http://creativecommons.org/licenses/by-nc-nd/4.0/).

1. Introduction

Humankind extracts valuable minerals from the Earth's crust to support the manufacturing of different products. However, mining activities produce waste such as tailings, waste rocks, dust and treated or untreated industrial wastewater, often causing significant adverse impact on the local environment and population health when proper management or mitigation strategies are not in place (Duruibe et al., 2007; Bhuiyan et al., 2010; Li et al., 2014; Oberholster et al., 2017; Atangana and Oberholster, 2021; Zhou et al., 2020). Demand for mineral resources is continuously increasing driven largely by population and economic growth, which leads to a corresponding increase of environmental costs (GAIN, 2020). There is a need to handle historical mine pollution issues and concurrently to learn from these cases for minimizing the environmental impacts of new mining activities in the future. In order to achieve this goal, it is necessary to understand how mine pollution is transported from its source through a catchment. Many studies note the importance of trace metal transported by suspended sediment in a catchment and highlight that this might be an important path for pollution transport from the mine area to the downstream aquatic system (Song et al., 2010; Thorslund et al., 2012b; Hu et al., 2015). However, the total metal concentration measured in soil or suspended sediment provides limited information regarding the mobility and bioavailability of these trace metals as only a small portion of the solid phase is geochemically active and able to rapidly exchange with solutes in water (Degryse et al., 2009; Jeng and Singh, 1993; Guzman-Rangel et al., 2020). Although a relatively large fraction of metal is in a non-active state it may undergo slow reactions and weathering, becoming reactivated especially under relatively acid aquatic or soil environments (Thornton, 1995; Rieuwerts et al., 1998; Hamon et al., 2002; Degryse et al., 2009). A key concern is to what extent the non-active phase metal in suspended sediment can (potentially) become bio-available under a changing environment over time. Therefore, the quantification of the fraction of labile and non-active phase trace metal (TM) is crucial for pollution risk management, but very few studies have dealt with this separation at the catchment scale.

TM migration from upland sources to the catchment outlet involves both physical movement (with water and sediment) and geochemical transformation processes, in addition to complex interactions among hydrological processes, soil erosion, sediment transport and geochemical reactions (Bilotta and Brazier, 2008; Kirchner and Neal, 2013; Li et al., 2019; Charlesworth et al., 2011; Yang et al., 2014). To fully quantify the complex mechanisms of TM transport at catchment scale through observation, a large number of measurements would be necessary. However, some measurements are intrinsically difficult and highly demanding of time and resources. Therefore, models become an interesting surrogate of measurements to characterize pollution dynamics across catchments and can be used as virtual laboratories to support the evaluation of potential risks and management practices in improving regional water quality (Borah and Bera, 2004; Daniel et al., 2011; Yuan et al., 2020; Botter et al., 2021). Various catchment-scale TM transport models were developed since the 1970s, which have their own advantages and weaknesses. These models are characterized by different levels of complexity in relation to their ability to quantify hydrological and geochemical processes, as well as in terms of spatial variability of input parameters and temporal scales of model application. L-THIA (Lim et al., 1999) and N-SPECT/OpenNSPECT (Carter and Eslinger, 2004) are two representative simple models, which are built on empirical and statistical relationships between TM pollution loads, land use, rainfall, and runoff volume. They require very limited input data and simple calibration, but they cannot simulate detailed hydrological and physicochemical processes of TM transport. A group of more advanced models is characterized by coupling a simple geochemical transformation module to a process-based (semi-)distributed hydrological model. Two representative cases that specifically simulate TM are TREX, which combines a spatially distributed hydrological representation with a simple conceptual metal partitioning process (Velleux, 2005), and SWAT-HM (Soil Water Assessment Tools – Heavy Metal), which is a conceptual semi-distributed hydrological model to which a metal transformation module was added (Meng et al., 2018). However, the model structure of TREX limits its applicability as it can only be applied at event scale (Velleux et al., 2008). Due to its semi-distributed nature, SWAT-HM could not explicitly simulate TM transport pathways and connectivity across the catchment. Therefore, it may not easily be used for investigations when spatially variable soil erosion and hydrological processes influence polluted sediment redistribution on the hillslope through erosion and deposition. Moreover, the finest temporal resolution of SWAT-HM is daily scale whereas, depending on the spatial scale, the dynamics of some key processes are characterized by finer temporal resolutions. Furthermore, both models lack a TM transport component in the groundwater making them unsuitable to evaluate the aquifer TM contribution to a river. These two models are thus difficult to apply to catchments where aquifers play a dominant role in river discharge and solute contribution. At a higher level of complexity, catchment solute transport models are often a combination of a physically-based distributed hydrological model and a complex geochemistry model with multi-component reactions and rigorous thermodynamics and kinetics representations as, for example, the RT-FLux-PIHM model (Bao et al., 2017). Such models typically show a good capability in mechanistically reproducing the effect of individual process on hydrological or geochemical aspects of solute transport. However, large data input requirements and computational costs limit their applicability to medium-size and large catchments and to cases where extensive observational data is lacking.

Accordingly, the overall scope of this article is to introduce a state-of-the-art catchment scale hydrology-sediment-chemical modeling framework for better understanding the characteristic of TM pollution transport in highly perturbed catchments where both point and non-point pollution sources exist. For achieving this goal, a new spatially distributed chemical transport and transformation module was developed and integrated into the existing hydrological and sediment transport model TOPKAPI-ETH, where TOPKAPI stands for '**TOP**ographic **K**inematic wave **AP**proximation and **I**ntegration (Battista et al., 2020; Fatichi et al., 2015). To avoid over-parameterization and preserve a high computational efficiency that enables application to large catchments, the newly developed metal transformation module was designed to include only essential processes. Although simple, it still includes the most important physical and chemical processes for simulating TM transport in both hillslopes and river channels, and at short and long temporal scales. To demonstrate the model characteristics and its range of possible applications, we applied the model to a headwater catchment under the influence of long-term mining activities in the Hunan province of South China. The specific research questions we address are: 1) To what extent can a physically explicit fully distributed model simulate the dynamics of observed river metal flux in the dissolved and total phase as well as explain the spatial variability of C-Q relationships? 2) What is the chemical phase distribution of exported metal from the case study catchment at annual-scale? 3) Can the model identify the spatial hot spots of metal pollution sources and their key drivers in both the short and long term?

2. Materials and methods

2.1. Hydrological and sediment transport model

A distributed trace metal transport and transformation module was developed and integrated with the hydrological model TOPKAPI-ETH (Fatichi et al., 2015; Battista et al., 2020). TOPKAPI-ETH was chosen because of its spatially distributed nature and physically explicit representation of the major hydrology-sediment processes as well as a reasonable computational efficiency, which makes possible long-term simulation (several decades) with a relative high resolution (0.0025–1

km^2 grid cell size, hourly time step) even for relatively large catchment (>1000 km^2). The model is based on a regular square grid discretization in space and, by default, three vertical layers in the subsurface, conceptualizing a shallow and a deep soil layer as well as a groundwater storage (see Fig. 1-a). In TOPKAPI-ETH, surface and subsurface flow is simulated using the kinematic wave approximation, with resistance to flow given by surface roughness and soil transmissivity which is a function of soil hydraulic properties. Overland flow is generated by the saturation excess mechanism when soil water exceeds maximum soil water storage capacity (Dunne runoff) or by the infiltration excess mechanisms when rainfall intensity exceeds saturated hydraulic conductivity of the surface soil (Horton runoff). Soil moisture is depleted by evapotranspiration, lateral drainage and percolation to lower storage layers. The sediment module simulates soil erosion and transport of the mobilized sediment by overland flow on the hillslopes and is based on a transport capacity approach at the cell level. The sediment erosion/deposition rate is determined by the local transport capacity, which depends on the overland flow discharge and topographic properties (Battista et al., 2020). The suspended sediment transport in the river channel is simulated as purely advective and can account for sediment exchange between the riverbed and the water column through a user-controlled threshold of settling velocity. Both water and sediment transport related variables are solved analytically (Liu and Todini, 2002; Battista et al., 2020). A more detailed description of the model is available from Liu and Todini (2002), Liu et al. (2005), Fatichi et al. (2015), and Battista et al. (2020).

2.1.1. Trace metal transformation module

The general conceptual model of trace metal partitioning and transformation in soil layers is adapted from Degryse et al. (2009) with the simplification of lumping the free ions, M^{n+}, and dissolved complexes, ML, together as total metal in solution phase, M_{sol} (see Fig. 1-b). In this study, we are indeed more interested in catchment-scale TM mobility rather than its speciation in the solution phase. In this module, we consider two types of reactions based on their relative reaction rate and importance in modeling TM mobility at catchment scale. The first type of reaction is sorption, which is the most important and relatively fast process that affects metal mobility in the natural environment (Fetter, 2018; Krupka et al., 1999). The sorption process is simulated with the linear Freundlich adsorption isotherm that balance between TM labile solid phase and solution phase (see Fig. 1-b and c) (Bradl, 2004; Degryse et al., 2009). The second reaction type accounts for slower processes, namely fixation/slow releasing and inert parent material weathering, which are modeled with kinetic constants. Integrating several complex biochemical reactions into two general types allows keeping the modeling of reactions simple enough, so that the model remains parsimonious in terms of parameters, but it can still reproduce the major dynamic of TM mobility for both short- and long-term simulations. Specifically, the solid-liquid partitioning coefficient K_d^{lab} [m^3/kg] of sorption is defined as:

$$K_d^{lab} = \frac{M_l}{M_{sol}}, \tag{1}$$

and expresses the ratio between the labile metal concentration in the solid phase, M_l [kg/kg], and the total metal concentration in the aqueous phase, M_{sol} [kg/m^3]. The model of slow reactions between metal in non-labile and labile solid phase (see Fig. 1-b) follows Crout et al. (2006) and Buekers et al. (2008), who described these reactions as empirical, reversible, first-order kinetic processes according to equations:

$$\frac{dM_l}{dt} = -k_1 M_l + k_2 M_n, \tag{2}$$

$$\frac{dM_n}{dt} = k_1 M_l - k_2 M_n, \tag{3}$$

$$k_1 = \frac{1}{T_c^f} - \frac{a_1 - a_2 \cdot pH}{T_c^f}, \tag{4}$$

$$k_2 = \frac{a_1 - a_2 \cdot pH}{T_c^f} \tag{5}$$

where M_n [kg/kg] is the metal concentration in non-labile phase, k_1 [day^{-1}] is the constant reaction rate of transformation from labile to non-labile solid metal phase, k_2 [day^{-1}] is the constant reaction rate of

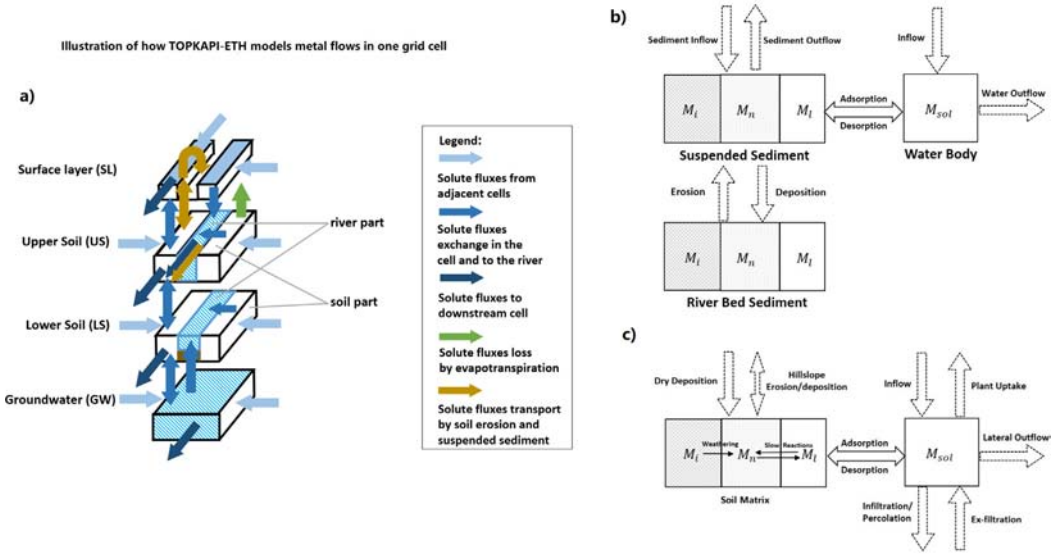

Fig. 1. a) Illustration of the conceptual scheme used by TOPKAPI-ETH to model trace metal flows by water and sediment in one grid cell. b) and c) Conceptual framework of trace metal transformation processes considered in the river compartment (b) and in the soil compartment (c), where M_i, M_n and M_l are trace metal in inert, non-labile, and labile solid phase respectively, M_{sol} is trace metal in aqueous phase including free ion and complex forms.

transformation from non-labile to labile solid metal phase, pH is the soil pH value, and T_c^f [day], a_1, a_2 are respectively the measured response time for the fixation reaction and the optimized regression coefficients to account for pH, based on the long-term incubation experiments data in diverse soils conducted by Crout et al. (2006) and Buekers et al. (2008). The weathering process of metal in the inert parent material of soil/waste rock is simulated with a constant rate, k_w [day^{-1}], that is assumed to slowly convert the inert phase TM, M_i [kg/kg], into non-labile phase, M_n [kg/kg], through the equation:

$$\frac{dM_n}{dt} = k_w M_i. \tag{6}$$

In the groundwater compartment, no specific metal solid phase classification is considered. Only a simple partitioning between TMs in a generic solid phase and dissolved phase is simulated by a user defined partitioning coefficient, K_d^{gw}.

2.1.2. Solute transport module in the hillslope and channel

The solute transport module of TOPKAPI-ETH computes the dynamic mass balance of solute within each storage compartments (i.e. channel, surface, soil, and groundwater) of a grid cell, which is driven by the hydrological and sediment transport processes (see Fig. 1-a). External sources can add or remove solutes in each storage compartments of each gird cell. The solute transport is modeled by the advection equation along topographically predefined flow directions identified by a D8 flow direction method in both surface and subsurface layers (O'Callaghan and Mark, 1984). The detailed numerical implementation of the solute transport module is discussed in Supplementary material Section 1. The model assumes that the solute concentration in dissolved or in solid phase is well mixed within each storage compartment of each cell and no residual or passive storage is considered in the model. In other words, the model only calculates the average concentration of a given solute in each compartment and for each time step. The specific solute transport continuity equations of different storage compartments in one grid cell, i.e. solute transport in the surface layer, soil layers, groundwater layer and river channel compartments, are elaborated in the next section and correspond to the transport processes depicted in Fig. 1-a.

2.1.2.1. Solute infiltration and lateral transport in surface layer. The dissolved solute in the rainfall or surface water can enter into the top soil layer through infiltration as well as flows to downstream cell through overland flow, which is governed by the following solute continuity equation:

$$\frac{\partial\left(C_{surf,i}V_{surf,i}\right)}{\partial t} = \sum F_{surf,i} + E_{surf,i} - \left(Q_{latout,i}^{surf} + Q_{infil,i}\right)C_{surf,i} \tag{7}$$

where $C_{surf,i}$ [kg/m^3] and $V_{surf,i}$ [m^3] are respectively the dissolved solute concentration in surface water and surface water volume, $\sum F_{surf,i}$ [kg/s] is the total incoming solute mass rate entering the active cell i from its upstream cells through surface runoff, $E_{surf,i}$ [kg/s] is the external source/sink term in the surface layer including the solute mass rate through precipitation, $Q_{latout,i}^{surf}$ [m^3/s] and $Q_{infil,i}$ [m^3/s] are the average lateral outflow rate and infiltration rate in the current calculated time step given by the hydrological module.

2.1.2.2. Soil solute percolation and lateral transport. The dissolved solute concentration in the soil layers can be altered by the incoming solute through percolation from its upper soil layer and incoming lateral solute flux through soil seepage. The soil solute concentration is governed by the solute continuity equation:

$$\frac{\partial\left(C_{soil,i}V_{soil,i} + S_{soil,i}^{l}M_{soil,i}\right)}{\partial t} = \sum F_{soil,i} + E_{soil,i} - \left(Q_{perc,i} + Q_{exf,i}^{soil} + Q_{latout,i}^{soil}\right)C_{soil,i} - E_{plant,i} \tag{8}$$

$$S_{soil,i}^{l} = K_d^{lab,soil} C_{soil,i} \tag{9}$$

where $C_{soil,i}$ [kg/m^3] and $V_{soil,i}$ [m^3] are respectively the dissolved solute concentration and the soil water volume of grid cell i, $S_{soil,i}^{l}$ [kg/kg] is the soil solid solute concentration in labile phase, $M_{soil,i}$ [kg] is the mass of soil matrix, $\sum F_{soil,i}$ [kg/s] is the sum of incoming solute mass rate through percolation from upper soil layer and through soil lateral flow from its upstream grid cells, $E_{soil,i}$ [kg/s] is the external source/sink term in soil water, $Q_{perc,i}$ [m^3/s], $Q_{exf,i}^{soil}$ [m^3/s] and $Q_{latout,i}^{soil}$ [m^3/s] are the average percolation, exfiltration, and lateral outflow rate of soil water in the current time step given by the hydrological module, $E_{plant,i}$ [kg/s] is the average solute mass uptake rate by plants in the current time step, which is calculated by the plant uptake component, and $K_d^{lab,\ soil}$ [m^3/kg] is the partitioning coefficient of the soil compartment.

2.1.2.3. Groundwater solute transport. The dissolved solute can travel in the groundwater through lateral groundwater flow as well as by exfiltration if the groundwater compartment exceeds maximum storage capacity. This process is described by the solute continuity equations as:

$$\frac{\partial\left(C_{gw,i}V_{gw,i} + S_{gw,i}^{l}M_{gw,i}\right)}{\partial t} = \sum F_{gw,i} + E_{gw,i} - \left(Q_{exf,i}^{gw} + Q_{latout,i}^{gw}\right)C_{gw,i} \tag{10}$$

$$S_{gw,i}^{l} = K_d^{gw} C_{gw,i} \tag{11}$$

where $C_{gw,i}$ [kg/m^3] and $S_{gw,i}^{l}$ [kg/kg] are the solute concentration in aqueous and solid phase of groundwater compartment, $V_{gw,i}$ [m^3] and $M_{gw,i}$ [kg] are the groundwater water volume and solid matrix mass respectively, $\sum F_{gw,i}$ [kg/s] is the total incoming solute mass rate entering from upstream grid cells through groundwater lateral flow, $E_{gw,i}$ [kg/s] is the external source/sink term in the groundwater, $Q_{exf,i}^{gw}$ [m^3/s] and $Q_{latout,i}^{gw}$ [m^3/s] are, respectively, the average exfiltration and lateral outflow rate in the current time step given by the hydrological module, K_d^{gw} [m^3/kg] is the partitioning coefficient of the groundwater compartment.

2.1.2.4. Plant uptake of dissolved solutes. TOPKAPI-ETH calculates the total evapotranspiration (ET) with the Priestley-Taylor equation (Priestley and Taylor, 1972), which does not provide a mechanistic way to separate transpiration (T) from total ET. Therefore, a simple ratio coefficient ($\psi = T/ET = 0.7$) method was used for separating T from ET based on a long-term average value from multiple sites worldwide (Fatichi and Pappas, 2017). In the model, the dissolved solute loss due to plant uptake is assumed to occur only from the top soil layer and the derived transpiration rate is used as the driving force. Thus, the plant uptake of metals is calculated as $E_{plant,i}[kg/s] = \psi \cdot ET_i \cdot C_{soil,i}$.

2.1.2.5. Solute movement with hillslope erosion/deposition. The solute associated with sediment is moved by the soil erosion process that is driven by overland flow. The labile, non-labile, and inert solid phase metal that are attached to the eroded soil particles are assumed well mixed in their individual phases before moving to the downstream cell or be re-deposited in the current cell. The solute transport by soil erosion is thus governed by the following solute continuity equations:

$$\frac{\partial\left(S_{soil,i}^{l}M_{soil,i}\right)}{\partial t} = \sum F_{sedin,i}^{l} + E_{dry,i}^{l} + \left(Q_{depo,i} - Q_{ero,i} - Q_{sedout,i}\right)S_{soil,i}^{l} \tag{12}$$

$$\frac{\partial(S^n_{soil,i}M_{soil,i})}{\partial t} = \sum F^n_{sedin,i} + E^n_{dry,i} + (Q_{depo,i} - Q_{ero,i} - Q_{sedout,i})S^n_{soil,i} \quad (13)$$

$$\frac{\partial\left(S^i_{soil,i}M_{soil,i}\right)}{\partial t} = \sum F^i_{sedin,i} + E^i_{dry,i} + (Q_{depo,i} - Q_{ero,i} - Q_{sedout,i})S^i_{soil,i}, \quad (14)$$

where $S^l_{soil,i}$ was previously defined, $S^n_{soil,i}$ [kg/kg] and $S^i_{soil,i}$ [kg/kg] are the soil solute concentration in non-labile and inert phase, $F^l_{sedin,i}$ [kg/s], $F^n_{sedin,i}$ [kg/s] and $F^i_{sedin,i}$ [kg/s] are the incoming solute mass rate of labile, non-labile and inert phases associated with sediment entering the current cell i from its upstream cells respectively, $E^l_{dry,i}$ [kg/s], $E^n_{dry,i}$ [kg/s] and $E^i_{dry,i}$ [kg/s] are the mean solute dry deposition rate for labile, non-labile, and inert phase TM in the current time step, $Q_{depo,i}$ [kg/s], $Q_{ero,i}$ [kg/s], and $Q_{sedout,i}$ [kg/s] are the mean rate of sediment deposition, erosion, and lateral transport within the current time step given by the sediment module.

2.1.2.6. Channel solute transport and exchange with river bed. The river can receive dissolved solute and sediment associated solute from nearby upland and channel cells. The particulate solute in the riverbed can be exchanged with river suspended sediment if riverbed erosion/deposition occurs. The transport of river solute in dissolved and suspended sediment forms are modeled as purely advective. The solute transport continuity equation in a river channel reach is:

$$\frac{\partial C_{river,i}V_i}{\partial t} = E_{river,i} + E_{bed,i} + \sum F_{river,in} - Q_{out,i}C_{tot,i} - Q_{Depo,i}S_{sus,i} \quad (15)$$

with

$$C_{river,i} = C_i + C_{sus,i}\left(S^l_{sus,i} + S^n_{sus,i} + S^i_{sus,i}\right) \quad (16)$$

and

$$S^l_{sus,i} = K^{lab,river}_d C_{river,i}, \quad (17)$$

where $C_{river,i}$ [kg/m^3] is the total river solute concentration, including river dissolved solute concentration, C_i [kg/m^3], and sediment associated solute concentrations, $C_{sus,i}(S^l_{sus,i} + S^n_{sus,i} + S^i_{sus,i})$ [kg/m^3], where $C_{sus,i}$ [kg/m^3] is the suspended sediment concentration in the current time step and $S^l_{sus,i}$ [kg/kg], $S^n_{sus,i}$ [kg/kg], $S^i_{sus,i}$ [kg/kg] are the solute concentrations in labile, non-labile, and inert phase in the suspended sediment respectively, V_i [m^3] is the river water volume, $E_{river,i}$ and $E_{bed,i}$ [kg/s] are the sink/source term of river solute from external point source and from bed sediment erosion respectively, $\sum F_{river,in}$ is the total incoming solute mass rate entering the current channel cell i from the upstream cells, $Q_{out,i}$ [m^3/s] and $Q_{Depo,i}$ [kg/s] are the average river discharge and suspended sediment deposition rate within the current time step respectively, $K^{lab,\ river}_d$ [m^3/kg] is the partition coefficient for river suspended sediment/water.

2.2. Case study area

Baoshan catchment is a headwater catchment of Xiang River located in the Hunan province of south-central China, where modern mining started in the 1980s. Baoshan catchment is an urban-rural fringe area covering approximately 74 km^2 with elevation range of 89–479 m.a.s.l. and catchment slopes ranging between 0.008 and 1.167 [m/m] (mean = 0.156). It has a humid subtropical climate with a clearly distinguished dry season from August to January and rainy season usually starting from March and lasting until June or July with an average annual rainfall of 1507 mm and a mean temperature of 16.9 °C. The dominant soil type is red loam with a relatively low organic matter content. In the parts of the Baoshan catchment that are highly affected by industrial activities, a serious soil acidification has occurred in the past few decades due to the dual effect of acid rain and acid mine drainage from pyrite oxidation (Guttikunda et al., 2004). Such low soil pH environment facilitates the movement of trace metals from upland to nearby streams when rainfall occurs (Meng et al., 2018). The land use in Baoshan comprises seven main types, including forest, shrubs, grassland, agricultural land, water surfaces, urban and mine industry (see Fig. 2-a). The mountainous area is dominated by forest and shrubs, while the valley region comprises a large area of agriculture land (16 km^2) and urban/industry cover (2.3/1.6 km^2). The mine area is located in the upstream valley area of the catchment, which is characterized by distributed unprotected waste rock piles and mining related industry plants for ore flotation and wastewater treatment. The exploitation of mines and lack of environmental protection over past decades have caused serious environmental pollution problems in the Baoshan catchment (Dai et al., 2005). Waste rock piles along the river, release of industrial wastewater, and diffuse pollution caused by rainfall leaching and soil erosion have heavily deteriorated local water quality (Meng et al., 2018). Long-term irrigation with polluted river water as well as phosphate fertilizer application led to the accumulation of toxic metals, particularly Cd, in the agriculture land along the riverbank (Zeng et al., 2017; Fan et al., 2017; Dai et al., 2005).

2.3. Field sampling and measurement

2.3.1. River discharge and suspended sediment concentration

Two streamflow monitoring sites, M1 and M2 were set in the Baoshan river. M1 is located just downstream of the entire active mining area that includes the two mines, indicated as A and B in Fig. 2-a, and M2 is located downstream of M1 close to the catchment outlet. The water discharge at the two sites is estimated using a commercial cost-effective smartphone application developed by the Swiss company Photrack (https://discharge.ch/), which has been already successfully applied in both indoor lab environment and outdoor natural river system in various case studies (Carrel et al., 2019; Fehri et al., 2020). The application uses the built-in camera and accelerometer of the smartphone to optically measure open channel water level and surface velocity, from which the discharge is computed using the technique of Surface Structure Imaging Velocimetry (SSIV) (Lüthi et al., 2014; Carrel et al., 2019). The method requires calibration, which was performed at the beginning of the measurement campaign for relevant parameters of DischargeApp, e.g., the Manning-Strickler coefficient, in both M1 and M2. Further information regarding the monitoring sites is provided in the Supplementary material Section 2. The discharge measurement started in April 2019 and lasted until June 2020, with at least once a week frequency at both sites and with an increasing frequency, daily to half-day if rain events occurred. The river turbidity and suspended sediment concentration measurements took place only at the M2 site. The turbidity measurement covers the period from October 2019 to June 2020 by means of the OBS-3A Turbidity and Temperature Monitoring System device designed by Campbell Scientific with measurement rate of 2 *Hz* and hourly output record temporal resolution. In-situ river suspended sediment concentration was only measured from late March to June of 2020 during the rainy season at approximately weekly frequency following the standard of suspended sediment concentration procedure (*SSC*) of ASTM (1999).

2.3.2. Measurement of soil and river metal concentration

A total 43 shallow soil (0–40 cm depth) samples were collected in April 2019 with the sampling strategy of having a high density of sampling in the mining area and a relatively coarse density sampling in the downstream farmland area as well as in the undisturbed forested mountain region (Fig. 2-b). The collected soil samples were processed according to the single batch extraction method by Voegelin et al. (2003) to determine the metal concentration in different chemical phases. The river Zn and Cd concentration in M1 and M2 sites were measured between April 2019 and June 2020 at a weekly scale and with an increasing frequency during rainfall events. Before October

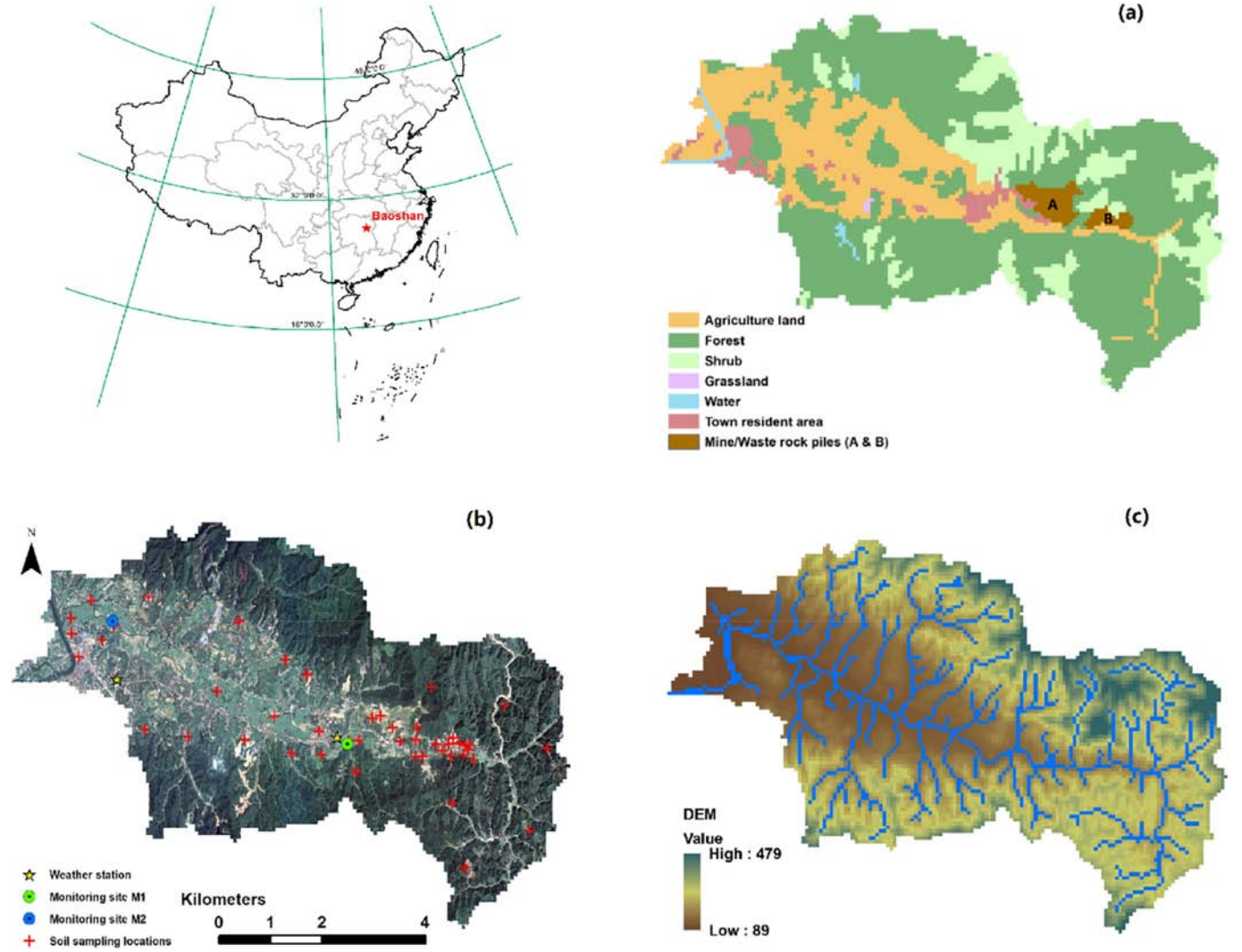

Fig. 2. (a) Land cover map at 30 m spatial resolution of the Baoshan Catchment in year 2018 (source: Data Center for Resources and Environmental Sciences, Chinese Academy of Sciences), The A and B areas are the mine/waste rock piles. (b) Satellite image of Baoshan catchment (source: Google Earth Pro 2020), soil sampling locations in April 2019 (plus symbol), and the two monitoring sites M1 and M2 (colored circles). (c) Digital Elevation Model (DEM) at 90 m spatial resolution of the Baoshan Catchment (source: Geospatial Data Cloud site, Computer Network Information Center, Chinese Academy of Sciences).

2019, only total metal concentration (dissolved + suspended sediment associated) was measured and afterwards both total and dissolved concentration were measured. The detail information about measurement protocols for soil and river water samples are available in the Supplementary material Section 3.

2.4. Water quality data analysis

Concentration-discharge (C-Q) relationships are an effective tool for interpreting river water quality data and they summarizes information of complex hydro-chemical processes occurring in the upstream drainage area (Musolff et al., 2015; Moatar et al., 2017; Botter et al., 2020). In this specific case, the C-Q relationship is expected to be largely controlled by the spatial and temporal availability of point and non-point pollution sources and their hydrological connectivity to the stream channel. In the entire measurement campaign from April 2019 to June 2020, we measured Baoshan river discharge as well as Cd and Zn concentration 97 times in the upstream M1 location and 107 times in the downstream M2 location. Specifically, the measurements contain 46 and 52 samples under 32 and 35 daily rainfall events with rainfall depth between 10 and 108.2 mm, and 51 and 55 samples under non-rainfall or relatively small rainfall events (daily rainfall depth smaller than 10 mm) for M1 and M2 respectively. We compute the C-Q relationships in a log(C)-log(Q) scale for both observed data and simulated data with the newly introduced metal transport model and classify the metal behaviors at the two monitoring stations, M1 and M2, on the basis of the log(C)-log(Q) slope values. The slopes are computed through linear regression and a Student's *t*-test (significance threshold α at 0.05) is applied to evaluate the statistical significance of having a slope different from zero. The C-Q relationship is defined as 'chemostatic' if the calculated slope is indistinguishable from 0 (p-value > 0.05), and as 'enrichment' behavior if the Student's *t*-test is significant (p-value < 0.05) and the slope larger than 0.

2.5. Model inputs and setup

2.5.1. Hydrology

The model was run at a spatial resolution of 90×90 m^2 that equals the resolution of the digital elevation model (DEM) (Fig. 2-c) used for deriving flow direction. The simulation covers the period from January 2018 to July 2020 with a temporal resolution of 1 h, where the first year is considered as a warm-up period and

the subsequent period is analyzed. The meteorological time-series inputs required to run TOPKAPI-ETH are hourly precipitation, air temperature, and cloud cover transmissivity. Hourly precipitation and air temperature data were available from three local weather stations managed by the Liuyang Meteorology Bureau (see Fig. 2-b). The station-level observed climate data were spatially interpolated with Thiessen polygon method. The hourly cloud cover transmissivity was derived from the hourly total cloud area fraction data product of M2T1NXRAD 5.12.4 by NASA. A land use map was obtained by resampling a 30×30 m^2 land cover product surveyed in 2018 by the Data Center for Resources and Environmental Sciences, Chinese Academy of Sciences (RESDC, http://www.resdc.cn) to 90 $\times$ 90 m^2. A new land use type named Mine/Waste rock piles (Fig. 2-a) was added to the resampled land cover map through visual interpretation of satellite images from Google Earth Pro and on-site verification in the study area. A 1:1,000,000 soil map of the catchment and related soil textural data, i.e., sand, silt, clay percentages, and soil density, were obtained from the Institute of Soil Science, Chinese Academy of Sciences (ISSCAS, http://www.issas.cas.cn). These soil textural data were used as input data to derive the residual and saturated water content and an initial value of saturated hydraulic conductivity of each soil type by means of the Rosetta pedotransfer functions (Schaap et al., 2001). Soil thickness map is not available, and a uniform soil thickness equal to 0.5 m was assumed for both upper and lower soil layers. The shallow groundwater layer was assumed to have a higher effective storage capacity in the valley area (i.e., cells with slope fraction < 0.05) than in the hillslope area (i.e., cells with slope fraction ≥ 0.05). The other parameters for running the hydrology module of TOPKAPI-ETH are listed in Table S3 and their values are obtained through calibration.

2.5.2. Sediment

The input parameters for running sediment component of TOPKAPI-ETH are α_{ero}, β and γ relating the overland flow transport capacity q_s to the overland flow q and the surface slope S ($q_s = \alpha_{ero} q^{\beta} S^{\gamma}$), and the E_{bed} (Eq. (15)) representing the exchange of sediment with the riverbed (Battista et al., 2020). The parameters β and γ are assumed spatially uniform and equal to 1.4, following the suggestion by Prosser and Rustomji (2000). The spatially distributed surface erodibility parameter α_{ero} is assumed to be proportional to the soil erodibility parameter K of the Universal Soil Loss equation (USLE) and the land use USLE parameter C through a constant α_1, specifically $\alpha_{ero} = \alpha_1 KC$. The distributed parameter C was derived from Yang et al. (2003) on the basis of the land use map, while the parameter K was calculated from basic soil properties, i.e. sand, silt, clay and soil organic carbon percentages, using the equation given by Sharpley and Williams (1990). The term E_{bed} is assumed equal to zero in this study, thus no fine sediment exchange between the riverbed and the suspended sediment is allowed. This assumption is based on the field observations carried out between April and July 2019, when no significant deposit of fine sediments was observed in the bed of the Baoshan river and bedrock and gravels were often exposed, except for few locations near bridges where sediments were deposited close to the bridge piers.

2.5.3. Trace metals transport and transformation

The input parameters for running TM transport and transformation module are listed in Table S3. The slow reactions related parameters, i.e. the k_1 and k_2 were estimated as spatially distributed parameters and calculated from measured soil pH and coefficients, T_c^f, a_1, and a_2 that were adopted from Crout et al. (2006) and Buekers et al. (2008). The weathering rate, k_w, is estimated only as a lumped parameter given by Bennett et al. (2000) and Starr et al. (2003). The $K_d^{lab,\ soil}$ values of collected soil samples were roughly estimated as the ratio between M_l and M_w. The soil sample pH was measured and then was used to compute a simple linear regression model (pH vs. $K_d^{lab,\ soil}$) for deriving a distributed map of K_d^{soil} as initial values (Degryse et al., 2009). As no information is available to estimate K_d^{gw}, we assumed that its initial values are the same as those estimated for the soil. With respect to point source inputs, two wastewater treatment plants detected through field investigations are the main point sources of pollutants in the Baoshan catchment, but only one plant has monitoring data of daily Cd load ([kg/day]) releases. The plant uptake process of trace metal was not considered in this study due to lack of data to constrain its magnitude. The initial soil TMs concentration map is estimated based on the field measurement data in Table S2. The inert fraction of the total non-active phase of Zn and Cd is assigned equal to 90% and 78% respectively based on the study of Meng et al. (2018) that analyzed 54 topsoil samples data collected in 2014 in the same study area (Supplementary material Table S2 in Meng et al., 2018). The lower soil concentration of Cd is estimated equal to 80% of the upper soil one based on the report of Zeng et al. (2017), which indicated a decreasing trend with depth of Cd concentration in local soil. A similar vertical variability was assumed also for Zn, as Zn is also typically not abundant in deep soil/rock. The groundwater solid trace metal concentration was estimated by the multiplication of the measured mean river metal concentration during the base flow period (Miller et al., 2017) and K_d^{gw}, which is assumed equal to the one of the soil. The external dry deposition hourly flux was calculated based on the values reported by Ke (2015) that equal 76.05 and 0.50 $mg/(m^2 \cdot yr)$ for Zn and Cd, respectively. We assumed that dry deposition falls on the upper soil with a rate constant for each time step and is uniformly distributed over the entire catchment.

2.6. Model calibration, validation and application

2.6.1. Model calibration and validation

The accurate simulation of metal transport in an anthropogenically disturbed, mine-impacted catchment is challenging because not only hydrological and sediment transport processes, but also various chemical reactions across different compartments play a role. Given the paucity of data and the related uncertainty, an automatic calibration could have been prone to artifacts more than a manual one. Despite characterized by subjectivity, manual calibration for complex physically based model can help reducing the risk of randomly combined parameter sets that fit the data well but lead to poor internal consistency of different processes (Boyle et al., 2000; Moradkhani and Sorooshian, 2009; Fatichi et al., 2015). Therefore, a manual trial-and error calibration method was applied. The hydrological simulation was calibrated with the measured discharge between April 2019 and October 2019 in sites M1 and M2, whereas the validation period used observation from November 2019 to June 2020 at same sites. The channel suspended sediment simulation was calibrated with the measured data of river turbidity and suspended sediment concentration between November 2019 and June 2020 in site M2, which covers the main rainy season of 2020, and no additional data for validation. The calibration period for the trace metal simulation of Zn and Cd was set from October 2019 to June 2020 in sites M1 and M2, during which total and dissolved river metal concentration were both measured, whereas the validation period was set between April 2019 and October 2019, when only total river metal concentration was measured at the same sites. The best fit was determined by two metrics of performance, the Nash-Sutcliffe efficiency, NSE, and the correlation coefficient, r, that are calculated using the simulated and measured discharge, suspended sediment flux, and metal flux (concentration) time series over the calibration period. The most sensitive parameters in influencing hydrology, sediment, and trace metal simulations as well as the detail calibration strategy are discussed in the Supplementary material Section 4. The values of all

parameters that were identified through manual calibration are summarized in the Table S3.

2.6.2. Numerical experiments

After confirming the model plausibility in simulating trace metal transport, we conducted several numerical experiments to show the model diagnostic and prognostic capability in helping understanding how specific artificial interventions or physicochemical process influences metal transport across the catchment. These experiments can also provide valuable information in terms of ecological risk assessment and in guiding pollution remediation strategies. In particular, we designed three numerical experiments, namely (i) we investigated the individual and combined effect of point and non-point sources in changing the C-Q relationships; (ii) we investigated the TM pollution generation hotspots in space and the dominant transport pathways; and (iii) we explored the importance of slow reactions in simulating metal transport at short and long temporal scales.

3. Results and discussion

3.1. Model calibration and validation results

3.1.1. Hydrology and sediment transport

The Fig. 3-a and b illustrate the observed and simulated discharge and suspended sediment flux (*SSF*) at the M2 location, whereas the performance of their corresponding hydrological indicators is summarized in Table 1. In general, at the M2 monitoring location, the simulation during both calibration and validation period shows very good performance in reproducing discharge dynamics and magnitude. Although the performance is slightly weaker for suspended sediment than for streamflow, the result is still encouraging. A relatively lower *r* value is obtained using turbidity rather than using *SSF* or *SSC*. This is mainly attributed to the measurement error induced by floating material, e.g., leaves or plastic bags, blocking the sensor measuring turbidity, which was observed in the field during low-flow periods. Given the strong anthropogenic disturbances in the upstream mining area, such

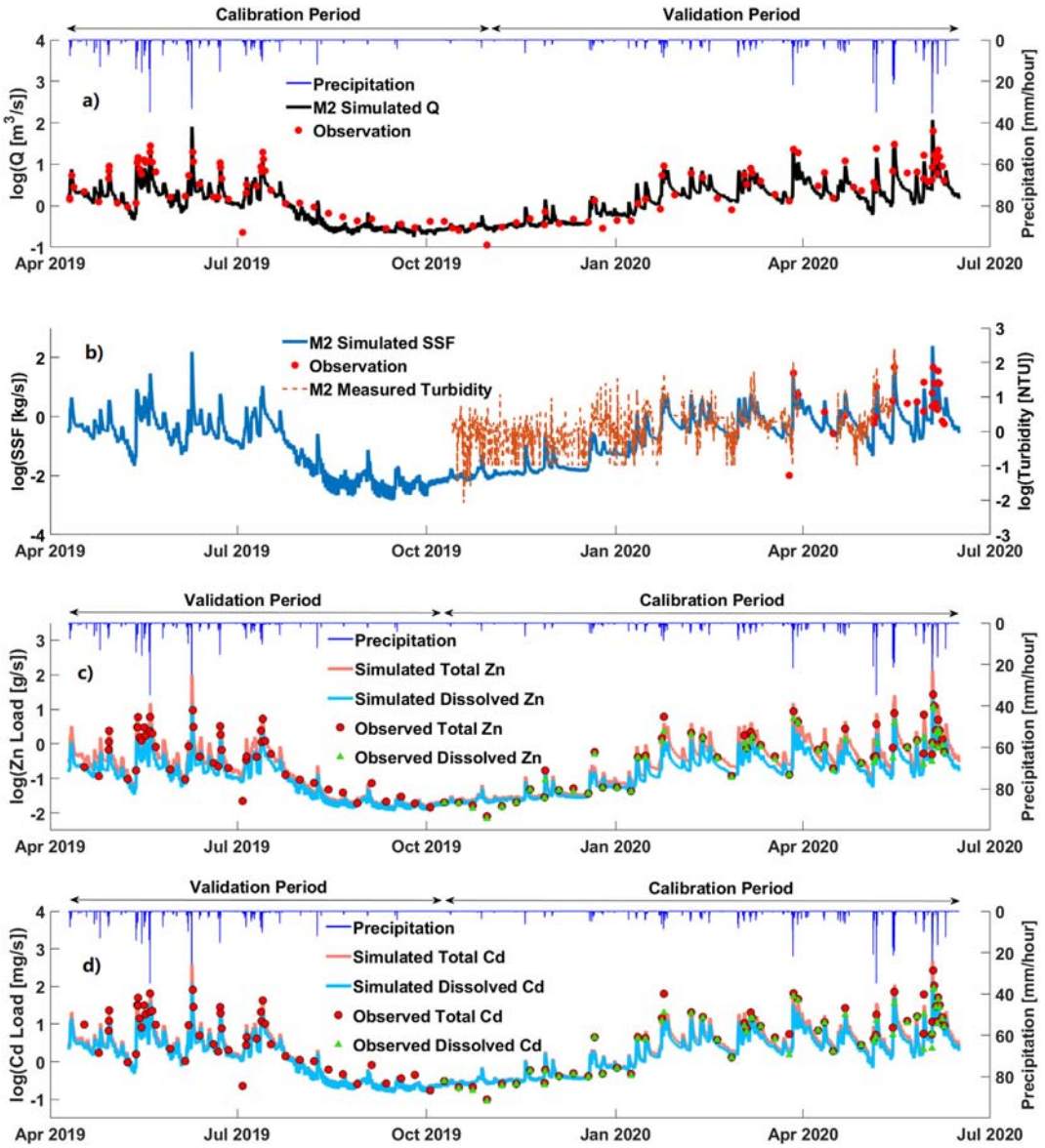

Fig. 3. Simulated and observed hydrology, sediment and trace metals dynamics at the M2 monitoring station between April 2019 and June 2020. a) Simulated and observed river discharge (*Q*) and observed precipitation; b) Simulated and observed suspended sediment flux (*SSF*) and measured river turbidity; c) and d) Simulated and observed Zn (c) and Cd (d) flux in total and dissolved phases and observed precipitation.

Table 1
Model performance metrics for simulated river discharge, suspended sediment, and trace metals fluxes at M1 and M2 monitoring points at hourly temporal resolution between April 2019 and June 2020 in terms of Nash-Sutcliffe efficiency (*NSE*) and correlation coefficient (*r*). The asterisk * represents the model performance in the scenario of adding one of the upstream Cd point sources to the base simulation scenario that only considers non-point pollution sources.

Location	Indicator	Hydrology		Suspended sediment		Zn flux			Cd flux		
		Q		SSF/SSC	Turbidity	Total	Dissolved	Total	Total	Dissolved	Total
		Calibration	Validation	Calibration	Calibration	Calibration	Calibration	Validation	Calibration	Calibration	Validation
M2	*NSE*	0.83	0.81	0.64/0.52	–	0.67	0.54	0.84	0.69/0.69*	0.57/0.57*	0.76/0.78*
	r	0.96	0.96	0.82/0.73	0.55	0.9	0.83	0.94	0.91/0.90*	0.85/0.83*	0.93/0.92*
M1	*NSE*	0.64	0.81	–	–	0.51	0.57	0.63	0.64/0.65*	0.62/0.65*	0.67/0.66*
	r	0.88	0.96	–	–	0.78	0.88	0.83	0.80/0.81*	0.87/0.89*	0.84/0.83*

as wastewater discharge, river channel lining and artificial canals, the model that is set up for simulating natural hydrological dynamics cannot fully capture the hydrological response in the drainage area of M1. The smaller and more impacted area of M1, amplifies the effects of disturbances, which are less relevant at M2, because M2 integrates more undisturbed area. This is the likely explanation of a slightly poorer simulation result observed at M1 (Fig. S1-a) compared to M2.

3.1.2. Trace metal transport

Fig. 3-c and d present the simulated Zn and Cd fluxes at M2 and their corresponding observed values. Overall, the simulated Zn and Cd fluxes in both dissolved and total phases during calibration and validation periods fit the observations reasonably well and reproduce their temporal dynamics and magnitude, as illustrated by the computed *NSE* and *r* values in Table 1. The seasonal pattern of metal transport dynamics is also well represented. The river metal load varies with the precipitation in response to changes in the leaching process: under dry or light rain periods, metals are mainly transported in the dissolved phase, but metal transport in the particulate phase plays a dominant role during heavy storm events due to soil erosion. The model performance at M1 (Fig. S1-b and c) is slightly worse than that at M2. Two possible reasons may explain the decline of performance simulation at M1: the first one is the relatively weaker performance in simulating the discharge at M1 compared to that at M2, the second is the lack of consideration, in these simulations, of point pollution from the two wastewater treatment plants just upstream of M1. In the base simulation, we indeed did not consider local point source pollution to avoid introducing additional uncertainty, as it is hard to have reasonable estimates of the flow rate and metal concentration (load) time series outputs from local wastewater treatment plants that are influenced strongly by daily mine production and climate conditions. The potential influence of point sources is further investigated through the comparison of the simulated and observed total metal concentration (*C*) and discharge (*Q*) relationship, as detailed in the following section.

3.2. Model ability to reproduce C-Q relationships

Observations of C-Q relationships (Fig. 4) reveal that Zn and Cd behave similarly at M1 and M2, but the relevance of 'enrichment' behavior is different at M1 and M2. At the upstream M1 monitoring location, both elements show an extremely weak (although significant) 'enrichment' behavior (p-value < 0.05) with calculated slopes values of 0.08 and 0.09 for Zn and Cd respectively, indicating that metal concentration is nearly invariant with discharge. From M1 to M2, the degree of 'enrichment' behavior for both elements increases significantly with calculated slope values raising to 0.3 and 0.24 for Zn and Cd respectively. This spatial variability of the observed C-Q relationships was not reproduced by the model. In both sites, the simulated slopes of Zn and Cd show strong

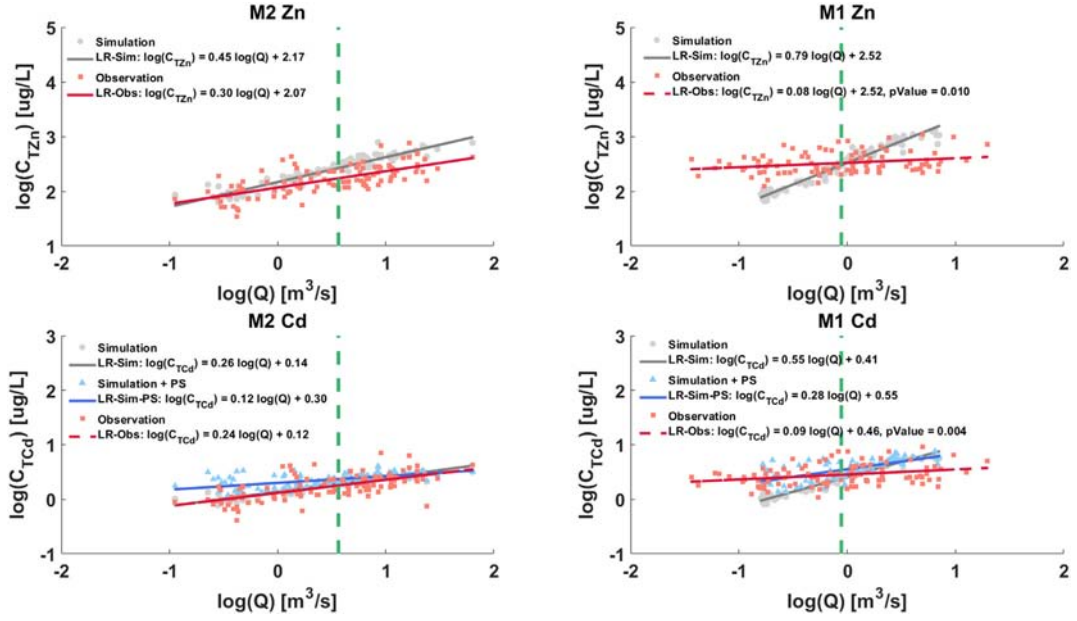

Fig. 4. Comparison of simulated and observed trace metal concentration (C) and discharge (Q) relationship in a log(C)-log(Q) scale and their linear regression results in terms of total Zn and Cd concentration at the M1 ($n = 97$) and M2 ($n = 107$) monitoring stations for the period between April 2019 and June 2020. The scenario of 'Simulation + PS' for Cd indicates the effects of adding one upstream Cd point source input, which is not included in the base simulation scenario that only considers non-point pollution sources. The vertical dashed green line indicates the median discharge.

'enrichment' behavior with a magnitude in M1 larger than in M2 (Fig. 4). An obvious underestimation of Zn and Cd concentrations exists at M1 during low-flow periods, although such underestimation becomes less relevant at M2 (Fig. 4). We argue that this is likely due to the contribution of point-pollution sources to the total river metal flux determined by the wastewater effluents, which are remarkable during low-flow conditions and are not considered in the simulations. The influence of these wastewater effluent contributions to total streamflow is not obvious at M2, because it gradually decreases from M1 to M2, due to the increasing drainage area without additional point sources.

To confirm such an explanation, we carried out a supplementary numerical experiment. Using the same parameterization of the base simulation scenario, we added the only available point source input data, i.e., Cd from one wastewater treatment plant to check how such additional pollutant source influences the Cd C-Q relationship at the two monitoring points. Although the simulated slope of Cd in M1 in this simulation is still larger than the observed one, the underestimation of its concentration during low-flow conditions is less severe as proved by the decrease of the log(C)-log(Q) slope from 0.55 to 0.28 (Fig. 4). Similar findings regarding the effect of anthropogenic point sources in modifying water body C-Q relationships and elevating pollutant concentrations during low-flow period are also discussed by Zhang (2018) and Kibuye et al. (2020). The effect of neglecting point pollution sources is hard to notice during peak flows since in these conditions diffused pollution sources become the dominant contributor in releasing metal to the river, especially in the analyzed case study, where soil is heavily polluted. If the interest is purely on the total load, the error induced by neglecting the point source contributions can be ignored as indicated by the performance (*NSE* and *r*) of simulations, which do not exhibit obvious differences, as shown in Table 1. This is because in the catchment the variation of river discharge between low and high flow conditions is in the order of ~500 times, which is far larger than that of the metal concentration, which changes of a factor ~ 10. Similar findings have been observed in many other catchments around the world, especially in agriculturally managed catchments, where only very small variability in stream chemistry has been observed compared to variability in river discharge (Godsey et al., 2009; Basu et al., 2010; Botter et al., 2020). However, in small drainage areas where spatially distinct anthropogenic point sources dominate, this error might be significant, especially in dry periods and low-flow conditions. Despite the discrepancy at M1 between the C-Q relationship obtained from observations and from simulations, the overall good agreement between the simulated and observed metal fluxes and the good agreement of the C-Q relationships for Cd and Zn at M2, suggest that the newly developed TM transport module in TOPKAPI-ETH can be a powerful diagnostic and prognostic tool, which can act as complement, and in some cases as surrogate, of rare and difficult measurements thus contributing to better understanding of the space-time metal dynamics at catchment scales.

3.3. Trace metal export in different chemical phases

Quantification of metal flux in different chemical phases coming from polluted regions can provide important information on analyzing potential risks and guiding pollution remediation efforts. To demonstrate the model capability to characterize the metal export in different chemical phases, we use the simulation results of 2019 as an example, the rainy period of which starts from January with a monthly total precipitation of about 120 mm and lasts until the end of July. As shown in Fig. 5-a and c, both simulated Zn and Cd show an obvious seasonal export pattern with around 97% and 95% of the yearly load of Zn and Cd exported during this rainy period. The remaining amount is exported in the dry period (August to December) and is transported mainly in dissolved phase, since no soil erosion occurs in this period. During the rainy season, the transport of Cd in the dissolved phase still plays a dominant role, but the transport in the particulate phase can still reach up to 29%. Conversely, Zn transport is dominated by the particulate phase through soil erosion, reaching nearly 62% of total Zn export within the rainy season. In the very wet month of June, the particulate metal flux contribution can even reach 74% and 44% of total metal export amount for Zn and Cd, respectively. Accordingly, a significant increase of the particulate metal fraction in the river during storm events is indicative of the importance of erosion for releasing metals from hillslopes to river. Conversely, a dominant contribution of the dissolved fraction, as it is still the case for Cd in the Baoshan catchment, points at risks associated with the high bioavailability of the Cd.

Moreover, metals transported in the particulate phase can potentially induce toxic effects to downstream aquatic ecosystem, when TMs absorbed to suspended sediment undergo phase transformation

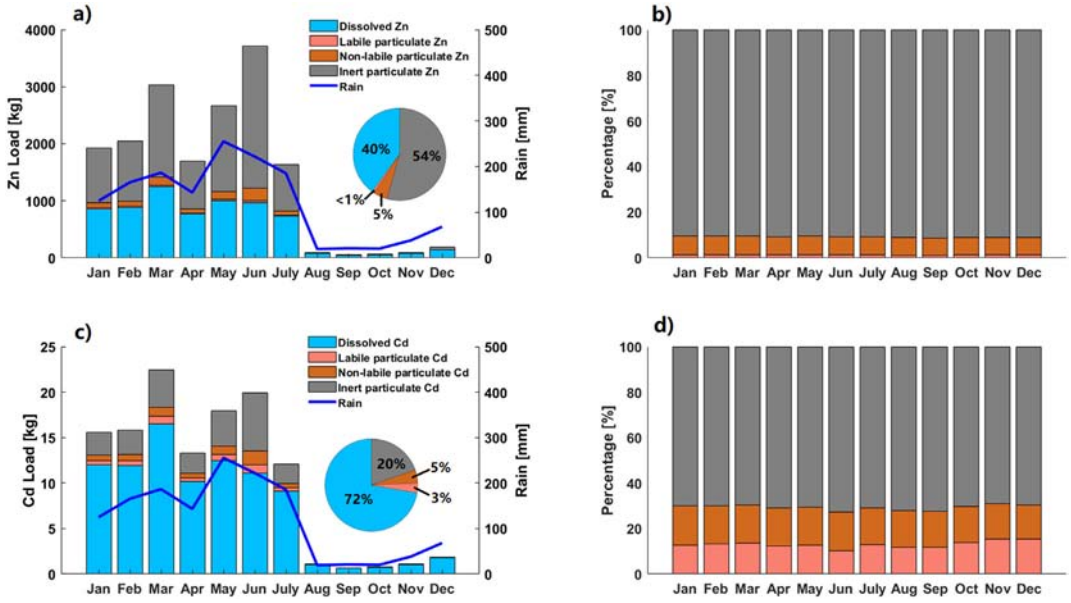

Fig. 5. Simulation results of monthly Zn and Cd flux from the Baoshan catchment in different chemcial phases for the year 2019. Subplots a) and c) show the composition of the Zn and Cd loads separated in the dissolved phase and different particulate phases; subplots b) and d) indicate the percentage of the particulate metal flux phases with different reactivity.

and become bioavailable (Tarras-Wahlberg et al., 2001; Khazheeva et al., 2008; Thorslund et al., 2012a). The newly developed TM transport module in TOPKAPI-ETH represents in this respect an advancement in the catchment-scale metal transport model landscape, as it takes solid metal phases classification and transformation into consideration in both upland and channel processes, thus providing the possibility to analyze the spatial and temporal distribution of solid metal phases with different reactivity along the river network. For instance, in the simulation result of year 2019, the inert metal percentage of Zn and Cd accounts for respectively 90% and 71% of the total solid metal in the exported suspended sediment (Fig. 5-b and d). From the model results, although Zn has a higher percentage of metal export to downstream through suspended sediment (60%) than that of Cd (28%), only a very small portion of particulate Zn is in labile and non-labile phase (10%) while for Cd this is 29%. The phase distribution of metals adsorbed to suspended sediment is not only determined by the solid metal phase distribution of the source, e.g., the composition of polluted soils and mine waste, but also by the mutual transformations among metal phases over time, which is controlled by the soil chemical environment, such as soil *pH*. In such a case, Cd in suspended sediments could be easier to transform into a bioavailable state than Zn, potentially providing adverse impacts to downstream aquatic ecosystems.

3.4. Identification of spatial trace metal transport hotspots

The identification of hotspots of metal pollution and the quantification of metal fluxes in different transport pathways is important for pollution control and design of remediation plans. The spatially distributed nature of the newly developed TM module and its explicit simulation of the connectivity allow identifying hotspots and their connectivity to the river network, in turn making possible the design of targeted prevention measures and remediation actions in space and across compartments. This model capability is particularly interesting, as the TM transport pathways may vary significantly in dry and wet periods due to different

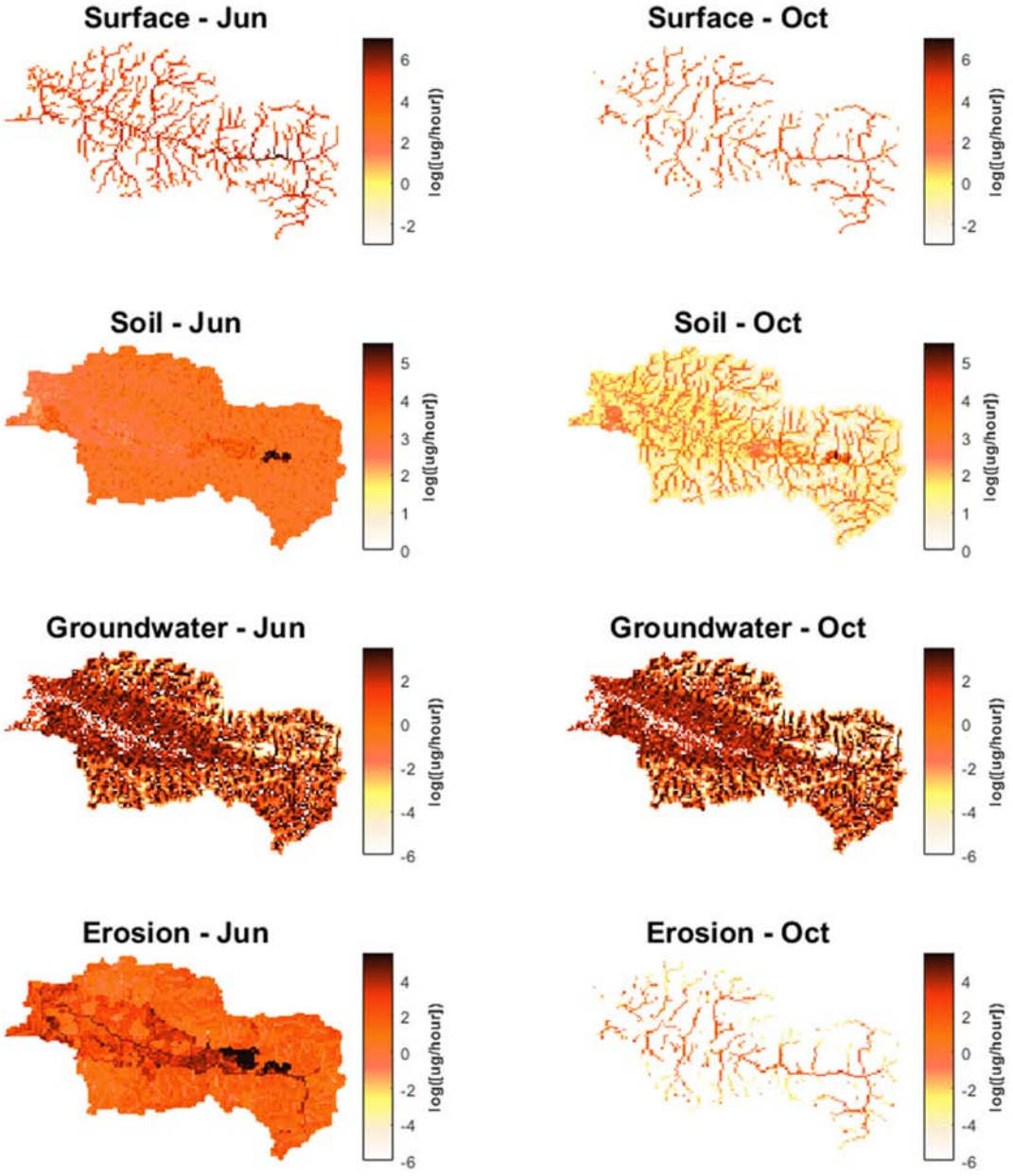

Fig. 6. Spatial distribution of average Cd flux transported through surface water flow, soil water lateral flow, groundwater flow and hillslope erosion in the wettest (June) and driest (October) month of year 2019.

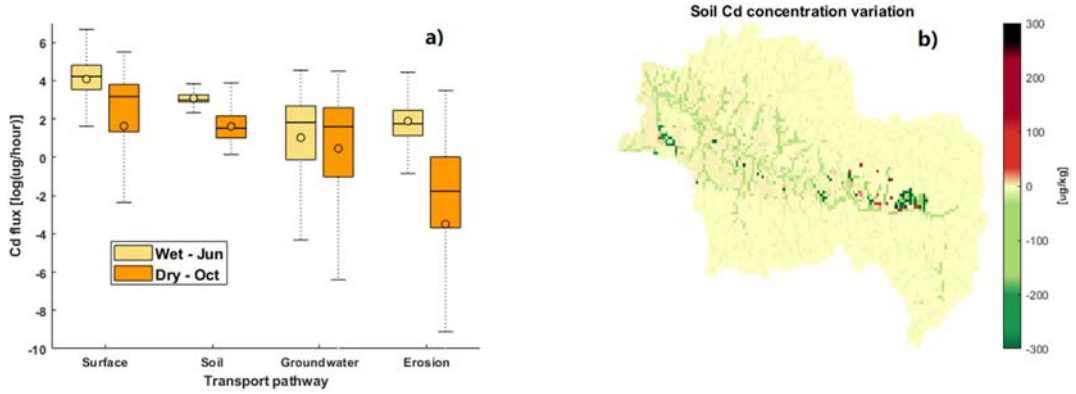

Fig. 7. a). Statistics of Cd fluxesover the entire catchment through different transport pathways in the wettest (June) and driest (October) month of the year 2019; b). Spatial distribution of soil Cd total concentration variation during the year of 2019, a positive(+)/negative(−) value indicates increased/decreased soil Cd concentration.

hydrological conditions. To demonstrate this capability, we investigate this point by analyzing the spatially distributed monthly average Cd flux, which is transported in the dissolved phase through overland flow, soil lateral flow, groundwater flow and in the particulate phase by soil erosion in the wettest (June) and driest (October) month of 2019 (see Fig. 6). In general, the transport of dissolved Cd by overland flow and soil water plays a dominant role compared to that of groundwater flow (Fig. 7-a). The transport of Cd through surface flow has a much higher transport capacity and connectivity in the wet period than in the dry period as it is evident from the denser Cd flux network in June than in October (see Fig. 6). Moreover, the hotspots of overland Cd flux concentrate in the highest order river reaches due to cumulative effects. During the wet period, the simulated Cd flux in soil shows a diffusive transport pattern with a well recognizable peak in the waste rock pile area, due to elevated water effective saturation in the entire catchment. However, in the dry period the transport of dissolved Cd in soil through the hillslopes is limited due to low soil water content and the transport is mainly occurring in the river network and in those valley areas, where soil saturation still occurs. In both dry and wet periods, the area containing the waste rock pile is evidently the hotspot for Cd source. This clearly highlights that, as expected, the mining area is the main pollution source for the entire catchment, in particular the Mine B area, where a relative high amount of labile Cd exists. This is evidently shown in the spatial map of soil Cd lateral transport flux during the simulation period of 2019 (Fig. 6). Through analyzing the spatial difference of total soil Cd concentration between beginning and end of 2019 (Fig. 7-b), an obvious Cd concentration decrease is observed in the area of Mine B, while a corresponding enrichment of Cd is observed in the channel area nearby. Due to a relatively low labile metal fraction in Mine A (see Table S2) compared to Mine B, no obvious hotspot is conversely observed there during the one-year simulation. However, if acid soil environment conditions persist, Mine A may become a long-lasting metal pollution source because of the large fraction of its non-labile Cd source, which may slowly transform into labile phase with time. The simulated hotspot of Cd flux through soil erosion concentrates in the mining and agricultural area with steeper slopes and frequent overland flow. In these areas a high soil erodibility exists due to the joint effect of land use type, soil properties, and topography. During the dry months, only a very low amount of soil erosion induced Cd transport was simulated close to the river channel where overland flow occurs due to exfiltration.

3.5. The role of slow reactions on long-term metal mobility

Another important aspect of pollution prevention and mitigation measures of mine waste is the understanding of the impact of slow reactions, as these can become, for instance, a long-term threat after decommissioning the mine if remediation measures are not implemented. To demonstrate the capability of the newly developed model of investigating the role of slow reactions (SRs, e.g. fixation/slow release and parent weathering) in influencing metal mobility with a longer temporal perspective, we recombined cyclically the climate data (e.g. rainfall, temperature, and total cloud cover fraction) of the years 2018 and 2019 in order to generate a 20 years hourly meteorological forcing to be used for a long-term simulation with and without consideration of slow reactions. We assumed that, in the entire simulation period, the initial condition of TM pollution distribution is the same as the base scenario as discussed in section 2.5.3, that no new waste rock pile was added to the catchment and that a uniform distributed dry deposition with a constant value took place. Moreover, we assumed that the soil pH remains unchanged throughout the entire simulation with the same values and spatial distribution as outlined in Table S2. Finally, for both scenarios, we use Cd as a representative metal. To evaluate the long-term metal mobility, we calculated the catchment monthly amounts of dissolved Cd and labile particulate Cd released from hillslopes to the river. The differences between the two scenarios, with and without SRs, computed with respect to dissolved and labile particulate Cd fluxes are displayed in Fig. 8-a. Moreover, we computed the corresponding time series of catchment average soil labile Cd fraction of the total solid Cd over 20 years and the catchment average fixation/slow release rates as shown in Fig. 8-b. A negative rate indicates that at the entire catchment level there is a net flux of Cd transferring from labile to non-labile phase (fixation dominated period), while a positive rate indicates a net flux from non-labile to labile phase (slow release dominated period).

The SRs show limited influence on dissolved Cd transport for short-term simulation (around 5 years), while their effect on the mobility of the dissolved TM becomes gradually more important on longer time scales. For the entire catchment, during the "fixation dominated period" a negative value occurs for dissolved flux difference (Fig. 8-a), thus indicating that, if SRs are considered, less dissolved Cd is released from hillslopes to the river than in the case of neglecting SRs. During this period, SRs can reduce TM solubility and show a capability of natural attenuation of TM contamination. The simulated fixation trend in labile metal agreed with the findings from other field experiments of polluted soil with trace metal, pointing out that TMs in the labile phase may slowly decrease over time as metal solubility decreases (Crout et al., 2006; Buekers et al., 2008; Jalali and Khanlari, 2008). A more rapid decrease of labile Cd fraction is observed in the fixation dominated period when SRs dynamics are considered (Fig. 8-b), because the decrease of labile Cd is not only due to leaching process but also to fixation reaction. However, during the fixation dominated period, we still found large part of the catchment, such as the area of Mine A and the entire agricultural region, showing a positive SRs rate (Fig. 8-c). These are the areas where

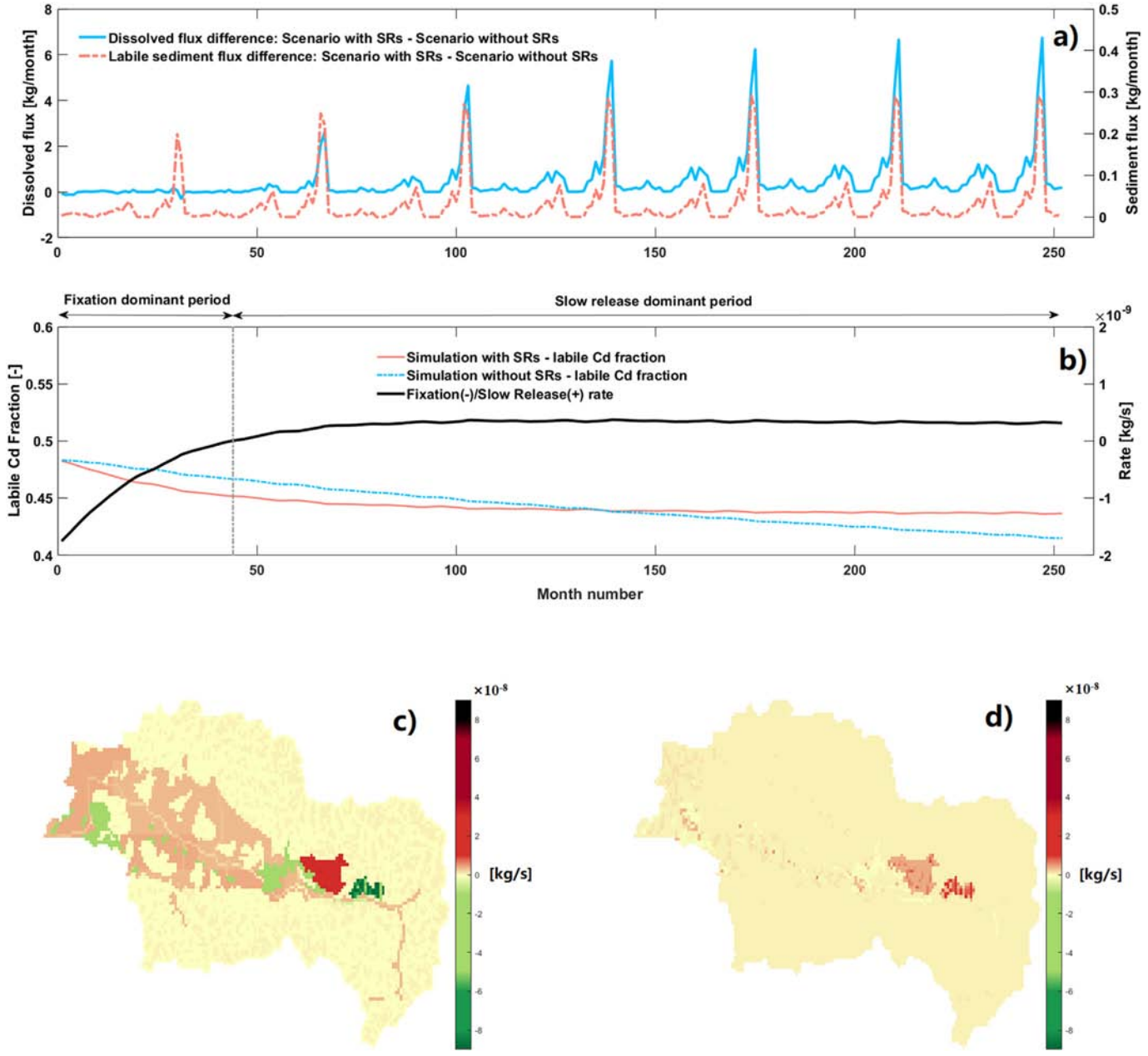

Fig. 8. a) The monthly difference of the Baoshan catchment Cd flux released from hillslope to channel between the simulation scenario with and without consideration of slow reactions (SRs): including dissolved flux (blue solid line) and labile particulate flux (carnation pink dashed line). b) Catchment average soil labile Cd fraction variation over time for scenario with (carnation pink solid line) and without (blue dashed line) consideration of slow reactions (SRs) as well as corresponding catchment mean SRs rate (black solid line). A positive/negative value (+/−) indicates an increase/decrease in labile metal concentration. The vertical grey dashed line indicates the time point at which the slow reaction rate transfers from negative (fixation dominated) to positive (slow release dominated). c) Average spatial distributed slow reaction rate over entire catchment in the fixation dominated period. d) Average spatial distributed slow reaction rate over entire catchment in the slow release dominated period.

soil erosion easily occurs, explaining why the labile sediment flux differences are positive even in the fixation dominated period (Fig. 8-a). With continuing depletion of the labile metal over time through leaching processes, the entire catchment transitions from a "fixation dominated period" to a "slow release dominated period", in which a positive value of the dissolved flux difference starts to emerge (Fig. 8-a), indicating that more dissolved Cd is released from hillslope to the river when SRs dynamics are considered. In the slow release dominated period, the decrease rate of the labile Cd in scenario with consideration of SRs is much slower than in the scenario without consideration of SRs (Fig. 8-b). This can be attributed to the fact that the labile Cd receives a continuous supply from its non-labile pool, thus creating, in areas such as mines, a stable long-term metal pollution source (see Fig. 8-d). This is especially the case under a very acid soil environment as in the Baoshan catchment. The simulations indicate that under an acid soil environment with labile metal continuously removed through rainfall leaching, the metal in non-active phase can slowly transform into the labile phase and increase metal mobility and bioavailability. A similar process was also found by other researchers through field observations and modeling studies (Hesterberg et al., 1993; Young et al., 2000; Hamon et al., 2002), reinforcing the plausibility of the model simulations.

4. Model limitation and uncertainties

The river discharge was only measured from April 2019 until June 2020. The case study region has a typical humid subtropical climate with a clearly distinguished dry and wet seasons, which leads to different discharge and suspended sediment flux export patterns in dry and

wet periods (Fig. S3-c and d). While using only one-year hydrological data for model calibration and validation is not ideal, it can still capture the regional rainfall-runoff response characteristics for both magnitude and seasonality as observed for a relative longer period. In fact, the statistics of measured data at the Shuangjiangkou hydrological station located 18 km downstream from the Baoshan catchment show that data of 2019 represent well seasonality of discharge and suspended sediment flux, as well as they cover their main variability over a relative longer period except for very few extreme flood events (Fig. S3-a and b). The river turbidity was measured for less than one hydrological year and most of suspended sediment concentration measurements were taken at heavy rainfall events during 2020. Using only such short period to calibrate sediment transport model introduce uncertainties in the obtained results. For this reason, we perform a sensitivity analysis (see Supplementary material Section 6) that show that erodibility parameters modify considerably the erosion magnitude and this has a big effect on simulated export of Cd and Zn in particulate phase, however, it has a very limited effect on the magnitude of the metal dissolved phase (Fig. S4-a and b). Within the particulate phase of Zn and Cd, the labile phase is more sensitive to the erodibility variations than the non-labile and inert phases, however the amount of labile phase was always very low compared to the other phases. Notably, erosion variability does not exert any obvious influence on the phase distribution of exported particulate Zn and Cd in the simulations (Fig. S4-c and d).

In the development of the reactive solute transport (metals) module, we assumed a reactive solute, e.g., a trace metal, that undergoes equilibrium exchange via linear adsorption/desorption reactions between the aqueous phase and the solid phase in the medium through which the fluid flows. In such a framework, the equilibrium partition coefficient, K_d^{lab}, of the species between the adsorbed and aqueous phases plays a critical role in controlling the retardation effect during transport. Using a partitioning coefficient, K_d^{lab}, to describe sorption is a concept often used in geochemistry, which is devoid of mechanistic interpretation and rather describes empirically the partitioning of total metal in its phases, aqueous (M_{sol}) and adsorbed on the medium (e.g. labile solid phase, M_l) through which the fluid flows (Stephen, 1999). This approach implicitly assumes that the reaction rate is fast enough to reach an equilibrium state between aqueous and adsorbed phase within each modeling time step. This is a reasonable assumption according to the relevant literature, especially for the metals like those addressed in this study, Zn and Cd, which have response times, T_c^f, of the order of 5 to 30 min (Ernstberger et al., 2002; Degryse and Smolders, 2005). These times are comparatively smaller than typical time-steps of catchment scale simulation, which generally vary between 1 h and 1 day. However, model applications for metals with very long sorption response time need to be considered carefully. The metal distribution between water and suspended sediment in rivers is also assumed to be in equilibrium as in many other river models (Garneau et al., 2015; Wool et al., 2006; Meng et al., 2018), however such assumption may not be realistic under quick flow conditions (Rubin, 1983). Concerning the slow reactions related parameters, because the observations are usually carried out over shorter periods than their typical time scales, one should consider the calibrated parameters and the resulting process dynamics as a coarse approximation of reality. In this study we only used the model for a sensitivity analysis to slow reactions. However, we suggest that long-term predictions of metal dynamics simulated with TOPKAPI-ETH, should be interpreted carefully in absence of more accurate parameter estimations and they should be used as a guideline rather than as precise quantitative predictions.

Theoretically, TOPKAPI-ETH due to its fully distributed nature can consider the influence of spatial heterogeneities of catchment processes on solute transport. However, in practical applications, the limited availability of detailed spatially distributed data often restricts the full exploitation of TOPKAPI-ETH capabilities. For instance, in the presented case study, K_d^{lab} and *pH* were measured using small volumes of soil collected at various locations covering all land use types within the study catchment. A simple linear regression model (*pH* vs. K_d^{soil}) was developed and used to derive a landuse-class-based distributed K_d^{lab} map in which the input variable, *pH*, was obtained as the average of measured pH of soil samples in each land use class. However, such land use class estimation of K_d^{lab} likely does not reflect the true heterogeneity within the catchment. Finally, it was found that long-term simulation results are influenced by slow reactions and are sensitive to some critical approximated initial conditions, such as soil metal concentration in different phases and soil *pH*.

5. Conclusion

A spatially distributed trace metal transport and transformation module was developed and integrated with the distributed hydrological model TOPKAPI-ETH. The presented model is able to simulate trace metal transport dynamics in the dissolved and particulate phases from various pollution sources potentially occurring at the catchment scale, such as in the case study presented in this article, which is influenced by long-term mining activity with both point and non-point pollution sources. The model was used to investigate the impact of mining on Cd and Zn release and transport, and to explain the reasons behind observed spatial variability of C-Q relationships within the catchment. The model results highlight the importance of considering metal phase classification in the catchment metal pollution management, as this allows to quantify the potentially bio-available metal phases in suspended sediment, as total metal adsorbed on suspended sediment is an incomplete and likely biased indicator to quantify trace metal pollution risk. Finally, we showed how slow reactions between the labile and non-labile phases have limited impact on metal transport over relatively short-term time horizons but exhibit more significant effects on the mobility of dissolved metal over longer periods. TOPKAPI-ETH, with its new trace metal module, is capable of simulating the relative importance of different hydrological and sediment transport processes on TM transport and can offer predictive capabilities in complex realistic settings to forecast effects of pollution sources and guide remediation strategies.

CRediT authorship contribution statement

Chunming Sui: Conceptualization, Methodology, Software, Formal analysis, Investigation, Writing – original draft, Visualization. **Simone Fatichi:** Conceptualization, Supervision, Writing – review & editing. **Paolo Burlando:** Conceptualization, Supervision, Writing – review & editing. **Enrico Weber:** Software. **Giulia Battista:** Software, Writing – review & editing.

Declaration of competing interest

The authors declare that they have no known competing financial interests or personal relationships that could have appeared to influence the work reported in this paper.

Acknowledgments

This study was supported by an ETH Zurich, Institute of Science, Technology and Policy (ISTP) Research Incubator Grant for the "Swiss Minerals Observatory Group". Thanks Dr. Lingfeng Zhou, Chinese Research Academy of Environmental Sciences, for the fruitful discussions and for providing soil trace metal data as well as to Dr. Scott Sinclair, ETH Zurich, for his help on code programming and testing. We specially thank Prof. Dr. Ruben Kretzschmar and Xu Fang of ETH Zurich for their help and guidance on the laboratory work in this study.

Appendix A. Supplementary data

Supplementary data to this article can be found online at https://doi.org/10.1016/j.scitotenv.2021.151473.

References

ASTM, 1999. Standard Test Method for Determining Sediment Concen-Tration in Water Samples, D3977-97. American Society for Testing AndMaterials, West Conshohocken, Pennsylvania.

Atangana, Ernestine, Oberholster, Paul J., 2021. Using heavy metal pollution indices to assess water quality of surface and groundwater on catchment levels in South Africa. J. Afr. Earth Sci. 182, 104254.

Bao, Chen, Li, Li, Shi, Yuning, Duffy, Christopher, 2017. Understanding watershed hydrogeochemistry: 1. Development of RT-flux-PIHM. Water Resour. Res. 53 (3), 2328–2345.

Basu, Nandita B., Destouni, Georgia, Jawitz, James W., Thompson, Sally E., Loukinova, Natalia V., Darracq, Amélie, Zanardo, Stefano, Yaeger, Mary, Sivapalan, Murugesu, Rinaldo, Andrea, 2010. Nutrient loads exported from managed catchments reveal emergent biogeochemical stationarity. Geophysical Research Letters 37 (23).

Battista, Giulia, Molnar, Peter, Burlando, Paolo, 2020. Modelling impacts of spatially variable erosion drivers on suspended sediment dynamics. Earth Surf. Dyn. 8 (3), 619–635.

Bennett, John W., Comarmond, M.Josick, Jeffery, John J., 2000. Comparison of Oxidation Rates of Sulfidic Mine Wastes Measured in the Laboratory and Field. Australian Centre for Mining Environmental Research Kenmore, Queensland.

Bhuiyan, Mohammad A.H., Parvez, Lutfar, Islam, M.A., Dampare, Samuel B., Suzuki, Shigeyuki, 2010. Heavy metal pollution of coal mine-affected agricultural soils in the northern part of Bangladesh. Journal of Hazardous Materials 173 (1–3), 384–392.

Bilotta, Gary S., Brazier, Richard E., 2008. Understanding the influence of suspended solids on water quality and aquatic biota. Water Res. 42 (12), 2849–2861.

Borah, Deva K., Bera, Maitreyee, 2004. Watershed-scale hydrologic and nonpoint-source pollution models: review of applications. Trans. ASAE 47 (3), 789.

Botter, Martina, Li, Li, Hartmann, Jens, Burlando, Paolo, Fatichi, Simone, 2020. Depth of solute generation is a dominant control on concentration-discharge relations. Water Resour. Res. 56 (8), e2019WR026695.

Botter, Martina, Zeeman, Matthias, Burlando, Paolo, Fatichi, Simone, 2021. Impacts of fertilization on grassland productivity and water quality across the european Alps under current and warming climate: insights from a mechanistic model. Biogeosciences 18 (6), 1917–1939.

Boyle, Douglas P., Gupta, Hoshin V., Sorooshian, Soroosh, 2000. Toward improved calibration of hydrologic models: combining the strengths of manual and automatic methods. Water Resour. Res. 36 (12), 3663–3674.

Bradl, Heike B., 2004. Adsorption of heavy metal ions on soils and soils constituents. J. Colloid Interface Sci. 277 (1), 1–18.

Buekers, Jurgen, Degryse, Fien, Maes, André, Smolders, Erik, 2008. Modelling the effects of ageing on Cd, Zn, Ni and Cu solubility in soils using an assemblage model. Eur. J. Soil Sci. 59 (6), 1160–1170. https://doi.org/10.1111/j.1365-2389.2008.01053.x.

Carrel, Maxence, Detert, Martin, Peña-Haro, Salvador, Lüethi, B., 2019. Evaluation of the DischargeApp: A Smartphone Application for Discharge Measurements. 2019. HydroSenSoft, Madrid, Spain.

Carter, H.J., Eslinger, D.L., 2004. Nonpoint Source Pollution and Erosion Comparison Tool (N-SPECT) Technical Guide. NOAA-CSC.

Charlesworth, Sue, De Miguel, E., Ordóñez, A., 2011. A review of the distribution of particulate trace elements in urban terrestrial environments and its application to considerations of risk. Environ. Geochem. Health 33 (2), 103–123.

Crout, Neil M.J., Tye, Andy M., Zhang, Hao, McGrath, Steve P., Young, Scott D., 2006. Kinetics of metal fixation in soils: measurement and modeling by isotopic dilution. Environ. Toxicol. Chem. 25 (3), 659–663.

Dai, T.G., Liu, X.H., Tong, Q.M., 2005. Comparison of environmental pollution at different period of time in qibaoshan mine area, Liuyang, Hunan. Min. Metall. Eng. 25 (6), 9–13.

Daniel, Edsel B., Camp, Janey V., LeBoeuf, Eugene J., Penrod, Jessica R., Dobbins, James P., Abkowitz, Mark D., 2011. Watershed modeling and its applications: a state-of-the-art review. The Open Hydrology Journal 5 (1).

Degryse, Fien, Smolders, Erik, 2005. Kineticspeciation of metal complexes in relation to metal mobility in soils. International Conference on the Biogeochemistry of Trace Metals.

Degryse, Fien, Smolders, Erik, Parker, D.R., 2009. Partitioning of metals (Cd Co, Cu, Ni, Pb, Zn) in soils: concepts, methodologies, prediction and Applications–a review. Eur. J. Soil Sci. 60 (4), 590–612.

Duruibe, J.Ogwuegbu, Ogwuegbu, M.O.C., Egwurugwu, J.N., 2007. Heavy metal pollution and human biotoxic effects. Int. J. Phys. Sci. 2 (5), 112–118.

Ernstberger, Helmut, Davison, William, Zhang, Hao, Tye, Andrew, Young, Scott, 2002. Measurement and dynamic modeling of trace metal mobilization in soils using DGT and DIFS. Environ. Sci. Technol. 36 (3), 349–354.

Fan, Yu, Zhu, Tingping, Li, Mengtong, He, Jieyi, Huang, Ruixue, 2017. Heavy metal contamination in soil and brown rice and human health risk assessment near three mining areas in central China. Journal of Healthcare Engineering 2017.

Fatichi, Simone, Pappas, Christoforos, 2017. Constrained variability of modeled T: ET ratio across biomes. Geophys. Res. Lett. 44 (13), 6795–6803.

Fatichi, Simone, Rimkus, Stefan, Burlando, Paolo, Bordoy, Roger, Molnar, Peter, 2015. High-resolution distributed analysis of climate and anthropogenic changes on the hydrology of an alpine catchment. J. Hydrol. 525, 362–382.

Fehri, Raed, Bogaert, Patrick, Khlifi, Slaheddine, Vanclooster, Marnik, 2020. Data fusion of citizen-generated smartphone discharge measurements in Tunisia. J. Hydrol. 590, 125518.

Fetter, Charles Willard, 2018. Applied Hydrogeology. Waveland Press.

GAIN, 2020. Global Aggregates Information Network. 2020. Global Aggregates Information Network.. https://www.gain.ie/.

Garneau, Cyril, Sauvage, Sabine, Probst, Anne, Sanchez-Pérez, José-Miguel, 2015. Modelling of trace metal transfer in a large river under different hydrological conditions (the Garonne River in Southwest France). Ecol. Model. 306, 195–204.

Godsey, Sarah E., Kirchner, James W., Clow, David W., 2009. Concentration–discharge relationships reflect chemostatic characteristics of US catchments. Hydrol. Process 23 (13), 1844–1864.

Guttikunda, Sarath K., Johnson, Todd M., Liu, Feng, Shah, Jitendra J., 2004. Programs to control air pollution and acid rain. Urbanization, Energy, and Air Pollution in China: The Challenges Ahead–Proceedings of a Symposium.

Guzman-Rangel, Georgina, Martínez-Villegas, Nadia, Smolders, Erik, 2020. The labile fractions of metals and arsenic in mining-impacted soils are explained by soil properties and metal source characteristics. J. Environ. Qual. 49 (2), 417–427.

Hamon, Rebecca E., McLaughlin, Mike J., Cozens, Gill, 2002. Mechanisms of attenuation of metal availability in in situ remediation treatments. Environ. Sci. Technol. 36 (18), 3991–3996.

Hesterberg, Dean, Bril, Jan, Castilho, P.Del, 1993. Thermodynamic Modeling of Zinc, Cadmium, and Copper Solubilities in a Manured, Acidic Loamy-sand Topsoil. Wiley Online Library.

Hu, Bangqi, Li, Jun, Bi, Naishuang, Wang, Houjie, Yang, John, Wei, Helong, Zhao, Jingtao, Li, Guogang, Yin, Xuebo, Liu, Ming, 2015. Seasonal variability and flux of particulate trace elements from the Yellow River: impacts of the anthropogenic flood event. Mar. Pollut. Bull. 91 (1), 35–44.

Jalali, Mohsen, Khanlari, Zahra V., 2008. Effect of aging process on the fractionation of heavy metals in some calcareous soils of Iran. Geoderma 143 (1–2), 26–40.

Jeng, Alhaji S., Singh, Bal Ram, 1993. Partitioning and distribution of cadmium and zinc in selected cultivated soils in Norway. Soil Sci. 156 (4), 240–250.

Ke, X.S., 2015. Pollution Characteristics and Source Analysis of Heavy Metals in Atmospheric Deposition in Chang-Zhu-Tan Area. Ocean University of China, Qingdao.

Khazheeva, Zinaida I., Tulokhonov, Arnold K., Yao, Rui, Weiping, Hu., 2008. Seasonal and spatial distribution of heavy metals in the Selenga River Delta. J. Geogr. Sci. 18 (3), 319–327.

Kibuye, Faith A., Gall, Heather E., Veith, Tamie L., Elkin, Kyle R., Elliott, Herschel A., Harper, Jeremy P., Watson, John E., 2020. Influence of hydrologic and anthropogenic drivers on emerging organic contaminants in drinking water sources in the Susquehanna River basin. Chemosphere 245, 125583.

Kirchner, James W., Neal, Colin, 2013. Universal fractal scaling in stream chemistry and its implications for solute transport and water quality trend detection. Proc. Natl. Acad. Sci. 110 (30), 12213–12218.

Krupka, Kenneth M., Kaplan, D.I., Whelan, G., Serne, R.J., Mattigod, S.V., 1999. Understanding Variation in Partition Coefficient, Kd, Values. Review of Geochemistry and Available Kd Values, for Cadmium, Cesium, Chromium, Lead, Plutonium, Radon, Strontium, Thorium, Tritium (3H), and Uranium. Volume II. EPA, p. 341 341.

Li, Zhiyuan, Ma, Zongwei, van der Kuijp, Tsering Jan, Yuan, Zengwei, Huang, Lei, 2014. A review of soil heavy metal pollution from mines in China: pollution and health risk assessment. Science of the Total Environment 468, 843–853.

Li, Tao, Sun, Guihua, Yang, Chupeng, Liang, Kai, Ma, Shengzhong, Huang, Lei, Luo, Weidong, 2019. Source apportionment and source-to-sink transport of major and trace elements in coastal sediments: combining positive matrix factorization and sediment trend analysis. Sci. Total Environ. 651, 344–356.

Lim, Kyoung Jae, Engel, Bernard A., Kim, Youngsug, Bhaduri, Budhendra, Harbor, Jon, 1999. Development of the long term hydrologic impact assessment (LTHIA) Www systems. Sustaining the Global Farm-Selected Papers From the 10th International Soil Conservation Organization Meeting, pp. 1018–1023.

Liu, Zhiyu, Todini, Ezio, 2002. Towards a comprehensive physically-based rainfall-runoff model. Hydrol. Earth Syst. Sci. 6 (5), 859–881.

Liu, Zhiyu, Martina, Mario L.V., Todini, Ezio, 2005. Flood forecasting using a fully distributed model: application of the TOPKAPI model to the upper xixian catchment. Hydrol. Earth Syst. Sci. 9 (4), 347–364. https://doi.org/10.5194/hess-9-347-2005.

Lüthi, Beat, Philippe, Thomas, Peña-Haro, Salvador, 2014. Mobile device app for small open-channel flow measurement. Proceedings of the 7th International Congress on Environmental Modelling and Software (IEMSs' 14), San Diego, CA, USA, pp. 15–19.

Meng, Yaobin, Zhou, Lingfeng, He, Shouliang, Chao, Lu., Ganlin, Wu., Ye, Wan, Ji, Peixi, 2018. A heavy metal module coupled with the SWAT model and its preliminary application in a mine-impacted watershed in China. Sci. Total Environ. 613–614 (12), 1207–1219. https://doi.org/10.1016/j.scitotenv.2017.09.179.

Miller, Matthew P., Tesoriero, Anthony J., Hood, Krista, Terziotti, Silvia, Wolock, David M., 2017. Estimating discharge and nonpoint source nitrate loading to streams from three end-member pathways using high-frequency water quality data. Water Resour. Res. 53 (12), 10201–10216.

Moatar, Florentina, Abbott, Benjamin W., Minaudo, Camille, Curie, Florence, Pinay, Gilles, 2017. Elemental properties, hydrology, and biology interact to shape concentration-discharge curves for carbon, nutrients, sediment, and major ions. Water Resour. Res. 53 (2), 1270–1287.

Moradkhani, Hamid, Sorooshian, Soroosh, 2009. General review of rainfall-runoff modeling: model calibration, data assimilation, and uncertainty analysis. Hydrological Modelling and the Water Cycle. Springer, pp. 1–24.

Musolff, Andreas, Schmidt, Christian, Selle, Benny, Fleckenstein, Jan H., 2015. Catchment controls on solute export. Adv. Water Resour. 86, 133–146.

O'Callaghan, John F., Mark, David M., 1984. The extraction of drainage networks from digital elevation data. Comput. Vision Gr. Image Process. 28 (3), 323–344.

Oberholster, Paul J., Botha, A.-M., Hill, Liesl, Strydom, Wilma F., 2017. River catchment responses to anthropogenic acidification in relationship with sewage effluent: an ecotoxicology screening application. Chemosphere 189, 407–417.

Priestley, Charles Henry Brian, Taylor, Robert Joseph, 1972. On the Assessment of Surface Heat Flux and Evaporation Using Large-Scale Parameters. Monthly Weather Review 100 (2), 81–92.

Prosser, Ian P., Rustomji, Paul, 2000. Sediment transport capacity relations for overland flow. Prog. Phys. Geogr. 24 (2), 179–193.
Rieuwerts, John S., Thornton, Iain, Farago, Margaret E., Ashmore, Mike R., 1998. Factors influencing metal bioavailability in soils: preliminary investigations for the development of a critical loads approach for metals. Chem. Speciation Bioavailability 10 (2), 61–75.
Rubin, Jacob, 1983. Transport of reacting solutes in porous media: relation between mathematical nature of problem formulation and chemical nature of reactions. Water Resour. Res. 19 (5), 1231–1252.
Schaap, Marcel G., Leij, Feike J., Van Genuchten, Martinus Th., 2001. Rosetta: a computer program for estimating soil hydraulic parameters with hierarchical pedotransfer functions. J. Hydrol. 251 (3–4), 163–176. https://doi.org/10.1016/S0022-1694(01)00466-8.
Sharpley, Andrew N., Williams, Jimmy R., 1990. EPIC. Erosion/Productivity Impact Calculator: 1. Model Documentation. 2. User Manual.
Song, Yinxian, Ji, Junfeng, Mao, Changping, Yang, Zhongfang, Yuan, Xuyin, Ayoko, Godwin A., Frost, Ray L., 2010. Heavy metal contamination in suspended solids of Changjiang river—environmental implications. Geoderma 159 (3–4), 286–295.
Starr, Michael, Lindroos, Antti-Jussi, Ukonmaanaho, Liisa, Tarvainen, Timo, Tanskanen, Heikki, 2003. Weathering release of heavy metals from soil in comparison to deposition, litterfall and leaching fluxes in a remote, boreal coniferous forest. Appl. Geochem. 18 (4), 607–613.
Stephen, D., 1999. The kd model, methods of measurement, and application of chemical reaction codes. Office of Environmental Restoration US Department of Energy, Washington, DC, p. 20585.
Tarras-Wahlberg, N.H., Flachier, A., Lane, S.N., Sangfors, O., 2001. Environmental impacts and metal exposure of aquatic ecosystems in Rivers contaminated by small scale gold mining: the Puyango River basin, southern Ecuador. Sci. Total Environ. 278 (1–3), 239–261.
Thornton, Iain, 1995. Metals in the Global Environment: Facts and Misconceptions. International Council on Metals and the Environment.
Thorslund, Josefin, Jarsjö, Jerker, Chalov, Sergey R., Belozerova, Ekaterina V., 2012a. Gold mining impact on riverine heavy metal transport in a sparsely monitored region: the upper Lake Baikal Basin case. J. Environ. Monit. 14 (10), 2780–2792. https://doi.org/10.1039/c2em30643c.
Thorslund, Josefin, Jarsjö, Jerker, Chalov, Sergey R., Belozerova, Ekaterina V., 2012b. Gold mining impact on riverine heavy metal transport in a sparsely monitored region: the upper Lake Baikal Basin case. J. Environ. Monit. 14 (10), 2780–2792.
Velleux, Mark L., 2005. Spatially Distributed Model to Assess Watershed Contaminant Transport and Fate. Colorado State University.
Velleux, Mark L., England Jr, John F., Julien, Pierre Y., 2008. TREX: spatially distributed model to assess watershed contaminant transport and fate. Sci. Total Environ. 404 (1), 113–128.
Voegelin, Andreas, Barmettler, Kurt, Kretzschmar, Ruben, 2003. Heavy metal release from contaminated soils: comparison of column leaching and batch extraction results. J. Environ. Qual. 32 (3), 865–875.
Wool, Tim A., Ambrose, Robert B., Martin, James L., Comer, Edward A., Tech, Tetra, 2006. "Water Quality Analysis Simulation Program (WASP)." User's Manual, Version 6.
Yang, Dawen, Kanae, Shinjiro, Oki, Taikan, Koike, Toshio, Musiake, Katumi, 2003. Global potential soil erosion with reference to land use and climate changes. Hydrol. Process. 17 (14), 2913–2928.
Yang, Zhongfang, Xia, Xueqi, Wang, Yaping, Ji, Junfeng, Wang, Dacheng, Hou, Qingye, Tao, Yu., 2014. Dissolved and particulate partitioning of trace elements and their spatial-temporal distribution in the Changjiang River. J. Geochem. Explor. 145, 114–123.
Young, S.D., Tye, A., Carstensen, A., Resende, L., Crout, N., 2000. Methods for determining labile cadmium and zinc in soil. Eur. J. Soil Sci. 51 (1), 129–136.
Yuan, Lifeng, Sinshaw, Tadesse, Forshay, Kenneth J., 2020. Review of watershed-scale water quality and nonpoint source pollution models. Geosciences 10 (1), 25.
Zeng, Hai-bo, Lei, Fan, Tong, Qian-ming, 2017. "The spatial-temproal evolution characteristic of cd pollution in the agricultural soil based on GIS". Journal of Anhui Agri. Sci. Kexue Chubanshe 45, 54–57. https://doi.org/10.13989/j.cnki.0517-6611.2017.06.056.
Zhang, Qian, 2018. Synthesis of nutrient and sediment export patterns in the Chesapeake Bay watershed: complex and non-stationary concentration-discharge relationships. Sci. Total Environ. 618, 1268–1283.
Zhou, Qiaoqiao, Yang, Nan, Li, Youzhi, Ren, Bo, Ding, Xiaohui, Bian, Hualin, Yao, Xin, 2020. Total concentrations and sources of heavy metal pollution in Global River and Lake water bodies from 1972 to 2017. Glob. Ecol. Conserv. 22, e00925. https://doi.org/10.1016/j.gecco.2020.e00925.